

**POLITECNICO DI MILANO**

School of Industrial and Information Engineering  
Master of Science in Mathematical Engineering:  
Quantitative Finance



**POLITECNICO**  
**MILANO 1863**

SINGLE BARRIER AND LOOKBACK  
OPTIONS: AN ANALYTICAL AND A  
NUMERICAL PRICING METHOD.

Supervisor: **Prof. Roberto Baviera**

Author: **Clarissa Elli**

ID: **876474**

Academic Year 2017-2018

# Contents

<b>Introduction</b>	<b>vi</b>
<b>1 The Wiener-Hopf method for option pricing</b>	<b>1</b>
1.1 Lévy Processes . . . . .	1
1.2 Complex Transforms . . . . .	2
1.2.1 Hilbert Transform . . . . .	3
1.2.2 Laplace Transform and Z-Transform . . . . .	4
1.3 Wiener-Hopf Factorization and Spitzer Identity . . . . .	4
1.3.1 Wiener-Hopf Factorization . . . . .	5
1.3.2 Spitzer Identity . . . . .	6
1.3.3 From Discrete to Continuous Time . . . . .	9
1.4 Lewis-like method for Option Pricing . . . . .	10
1.4.1 Single Barrier Option . . . . .	11
1.4.2 Lookback Option . . . . .	14
1.4.3 Digital Options . . . . .	15
1.5 Closed Formulas . . . . .	15
<b>2 Numerical Methods</b>	<b>18</b>
2.1 FFT Procedure . . . . .	18
2.2 Sinc Expansion for Hilbert Transform . . . . .	20
2.2.1 Toeplitz Matrix . . . . .	21
2.2.2 Exponential Filter . . . . .	22
2.2.3 Numerical Tests . . . . .	23
2.3 Trapezoidal Rule for the Inverse Laplace . . . . .	26
2.3.1 Euler Acceleration . . . . .	27
2.3.2 Numerical Tests . . . . .	27
<b>3 Results of the Wiener-Hopf method</b>	<b>29</b>
3.1 Pricing Procedure . . . . .	29
3.1.1 Brownian Motion model . . . . .	30
3.1.2 NIG Model . . . . .	33
3.2 Error Convergence . . . . .	35
3.3 Analysis of the Sinc Expansion . . . . .	37
3.4 Analysis of the damping parameter . . . . .	41

<b>4</b>	<b>A New Monte Carlo Method</b>	<b>44</b>
4.1	Brownian Motion . . . . .	44
4.2	Classical Monte Carlo Simulation . . . . .	45
4.3	Distribution of the Extrema . . . . .	46
	4.3.1 Joint Distribution of Brownian Motion and its Maximum	46
	4.3.2 Brownian Bridge and its Extrema . . . . .	47
4.4	New Monte Carlo Simulation for the BM model . . . . .	49
	4.4.1 Numerical results . . . . .	49
4.5	New Monte Carlo Simulation for NIG Model . . . . .	52
	4.5.1 Numerical Results . . . . .	54
<b>5</b>	<b>Conclusions</b>	<b>56</b>
	<b>Bibliography</b>	<b>59</b>

## Abstract

We describe two methods for the pricing of continuously monitored exotic options: an analytical method based on the Wiener-Hopf factorization and a Monte Carlo simulation approach. In the first case, making use of advanced mathematical elements such as the Hilbert Transform and the Inverse Laplace transform, we find a Lewis-like formula for option pricing. In the second method, we use the joint distribution  $(M_T, W_T)$  of the Brownian Motion and its maximum in order to modify the classic Monte Carlo simulation method and improve convergence for the pricing of path-dependent options. This technique has been generalized also to Lévy processes. In both cases, we consider two different Lévy models for the log-returns  $X_T$  of the underlying asset: a Brownian Motion and a NIG model. The aim is to price a single lower barrier option and a lookback option with fixed strike.

## Sommario

Questo elaborato si propone di descrivere due metodi per la valutazione di opzioni esotiche: uno analitico, basato sulla fattorizzazione di Wiener-Hopf, e un metodo Monte Carlo. Nel primo caso, utilizzando tecniche matematiche avanzate come la trasformata di Hilbert o la trasformata inversa di Laplace, si ottiene una formula di tipo Lewis per la valutazione di opzioni. Nel secondo approccio, viene introdotta la distribuzione congiunta del Brownian Motion e del suo massimo  $(M_T, W_T)$  per modificare il classico metodo Monte Carlo e migliorarne le caratteristiche di convergenza per opzioni path-dependent. Questa tecnica è generalizzata anche per processi di Lévy. In entrambi i casi, vengono considerati due diversi modelli di Lévy come dinamica per il logaritmo  $X_T$  del rendimento dell'azione sottostante: un modello di Brownian Motion e un modello NIG. Lo scopo è di valutare un'opzione barriera e un'opzione lookback con strike fissato.

# Introduction

Exotic Options are derivative instruments which are more complex than the commonly traded plain vanilla options. The pricing of this kind of options has been largely studied in the literature. In this work, we are going to focus on path-dependent options such as single barrier and lookback options, describing two different approaches for their pricing.

A first goal is to describe the method applied in Phelan et al. (2018), which is an analytical method for Lévy processes that exploits some advanced mathematical instruments, such as Complex Transforms. The idea of pricing plain vanilla options with this approach came out with Carr and Madan (1999) and then was developed by Lewis (2001). The criticalities of those methods have been studied and the extension to exotic options has been proposed in subsequent works, such as Sgarra et al. (2006), with the application of the Wiener-Hopf technique to the pricing of some exotic options under a Brownian Motion model. A wider mathematical description of the method can be found in Green et al. (2010), where the authors focus on the pricing of discretely monitored exotic options, such as barrier or lookback options, for general Lévy models. A more analytical discussion about the numerical methods applied is proposed by Feng and Linetsky (2008), while in Fusai et al. (2016) the application and the study of convergence for discretely monitored options is shown. However, this analytical method is very complex both from an theoretical point of view, since it involves complicated mathematical structures, such as the decomposition of Wiener-Hopf, and from a numerical point of view, exploiting numerical schemes with many criticalities, as we will see in this thesis.

For that reason, the second aim of this work is to propose a modification of the traditional Monte Carlo simulation scheme for two Lévy processes, the Brownian Motion model and the Normal Inverse Gaussian (NIG) model. The new numerical method exposed is based on the study about the simulation of the extrema of a Brownian Motion in the works of Becker (2010) and Alabert and Caballero (2018), but extending the approach also to the NIG model and analyzing the convergence of the error.

The main contribution of this thesis to the literature are:

- The analysis of the extension of the Wiener-Hopf method proposed in Phelan et al. (2018) for barrier options to continuously monitored lookback options, starting from the description of the method applied to a single barrier option. We also extend the result to American digital options.
- A discussion on the numerical convergence of the method proposed in terms of analyticity strip.

- The introduction of a new Monte Carlo method for the pricing of path-dependent options, in particular its extension to the Normal Inverse Gaussian model.
- A comparison between the convergence of the traditional Monte Carlo approach and the modified one.

This thesis is organized as follows. In Chapter 1, we describe the Wiener-Hopf method for exotic option pricing proposed in Phelan et al. (2018), with the definition of the mathematical elements involved and the derivation of the pricing formulas for a single barrier and a lookback option. Moreover, the Black & Scholes-like closed formulas for the options considered are summarized. In Chapter 2, the work proceeds in explaining the numerical methods exploited for the computation of the analytical expressions derived in the first chapter, with some numerical tests on known functions. In Chapter 3, the results of the analytical method are exposed; moreover, the analyticity strip for the models considered is studied. Chapter 4 describes the new Monte Carlo method, starting from the derivation of the distribution of the extrema for a Brownian Bridge, with the application to the Brownian Motion model and the NIG model.

# Chapter 1

## The Wiener-Hopf method for option pricing

In this chapter, we present the pricing method for exotic options studied by Phelan et al. (2018) and we see how this approach can be applied to continuously monitored single barrier and lookback options, considering also their digital versions. In particular, the mathematical objects that are used through this work are introduced in order to clarify the notation and the mathematical environment. First, the Lévy Processes and their main properties are described, as they are the processes analyzed in this work. Then, the definitions of Hilbert, Laplace and Zeta (Z-) Transform are given, since they are the fundamental instruments of the method presented, as they are widely applied in the Wiener-Hopf factorization. This particular factorization technique is first introduced in discrete time, following the approach of Green et al. (2010) and Fusai et al. (2016); finally, as shown in Phelan et al. (2018), we move from discrete to continuous time.

### 1.1 Lévy Processes

In probability theory, a Lévy Process is a stochastic process with independent and stationary increments.

**Definition 1.1** (*Lévy Process*). *A stochastic process  $X = \{X_t\}_{t \geq 0}$  is called a Lévy Process if it satisfies the following properties:*

- $X_0 = 0$  a.s.;
- $X_{t_{i+1}} - X_{t_i} \perp X_{t_{j+1}} - X_{t_j}$ , if  $[t_i; t_{i+1}] \cap [t_j; t_{j+1}] = \emptyset$ ;
- $\forall s < t$ ,  $X_t - X_s \sim X_{t-s}$ ;
- $\forall \epsilon > 0$ ,  $\forall t \geq 0$ :  $\lim_{h \rightarrow 0} \mathbb{P}(|X_{t+h} - X_t| > \epsilon) = 0$ .

The most well-known examples of Lévy Processes are the Brownian Motion and the Poisson Process. We are interested in the main properties of the characteristic function of a Lévy Process, therefore first we give the following definition:



**Definition 1.2** (*Characteristic Function*). Given a real random variable  $X$  with probability density function  $p_X(x)$ , its characteristic function is the function  $\widehat{p}_X : \mathbb{R} \rightarrow \mathbb{C}$  defined as:

$$\widehat{p}_X(z) = \mathbb{E}[e^{izX}] = \int_{\mathbb{R}} e^{izx} p_X(x) dx, \quad \forall z \in \mathbb{R}.$$

The characteristic function of a random variable uniquely identifies its distribution.

**Remark.** Notice that the characteristic function  $\widehat{p}_X$  is the Fourier transform of the probability density function  $p_X$ , since from the definition of Fourier Transform of a real-valued function  $f$ , we have:

$$\widehat{f}(z) = \mathcal{F}_{x \rightarrow z}[f(x)] = \int_{\mathbb{R}} f(x) e^{izx} dx, \quad \forall z \in \mathbb{R}.$$

Let's also recall the expression for the Inverse Fourier Transform:

$$f(x) = \mathcal{F}_{z \rightarrow x}^{-1}[\widehat{f}(z)] = \frac{1}{2\pi} \int_{\mathbb{R}} \widehat{f}(z) e^{-izx} dz, \quad \forall x \in \mathbb{R}.$$

**Proposition 1.1.** *The characteristic function of a Lévy Process can be written in the form:*

$$\Psi_X(z, t) = \mathbb{E}[e^{izX_t}] = e^{\psi(z)t},$$

where  $\psi(z)$  is called characteristic exponent and it's uniquely identified through the Lévy-Khincine triplet  $(\mu, \sigma, \nu)$  in the expression:

$$\psi(z) = i\mu z - \frac{1}{2}\sigma^2 z^2 + \int_{\mathbb{R}} (e^{iz\eta} - 1 - iz\eta \mathbb{1}_{[-1,1]}) \nu(d\eta).$$

Each parameter has a different interpretation:  $\mu$  represents the linear drift of the process,  $\sigma$  is the volatility of the diffusion part, while  $\nu(\eta)$  is the intensity of the Poisson process with jump size  $\eta$ . Many different models can be found under the Lévy Processes family by a different choice of the parameters. For option pricing, the risk-neutral measure in a framework with risk-free rate  $r$  and dividend yield  $q$  is recovered choosing  $\mu$  such that:

$$\mu = r - q - \frac{1}{2}\sigma^2 - \int_{\mathbb{R}} (e^{\eta} - 1 - i\eta \mathbb{1}_{[-1,1]}(\eta)) \nu(d\eta).$$

In this work, we will focus on two Lévy Processes: the Brownian Motion with drift and diffusion (BM) and the Normal Inverse Gaussian (NIG) model.

## 1.2 Complex Transforms

Transform techniques will be widely used in this work, in particular the Hilbert Transform, the Laplace Transform and its discrete version, the Z-Transform, exploited for the Wiener-Hopf factorization.

### 1.2.1 Hilbert Transform

The Hilbert Transform was introduced by David Hilbert in 1905, in connection to the Riemann problem, and it is mostly used in signal processing. In this work, the Hilbert transform will be used exploiting its relation with the Wiener-Hopf factorization, as explained in Kisil (2015). Here, we give the definition of the Hilbert Transform and we introduce the Plemelj-Sokhotsky relations as in King (2009).

**Definition 1.3** (*Hilbert Transform*). *The Hilbert Transform on the real line of a function  $f$  is defined as:*

$$\mathcal{H}[f(x)] = P.V. \frac{1}{\pi} \int_{\mathbb{R}} \frac{f(y)}{x-y} dy,$$

where  $P.V.$  denote the Cauchy Principal Value (c.f. King (2009, p. 2)).

**Remark.** Notice that the expression of the Hilbert Transform can be expressed through the convolution:

$$\mathcal{H}[f(x)] = P.V. \frac{1}{\pi x} * f(x). \quad (1.1)$$

We now derive a result for the computation of the half-range Fourier transforms of a function  $f$ , making use of the relations described in King (2009) between Hilbert and Fourier Transforms, in order to get the Plemelj-Sokhotsky relations as in Phelan et al. (2018).

**Proposition 1.2.** (e.g. Phelan et al. (2018, p. 213)) *The Fourier Transforms of the positive and negative part of a function  $f$  (i.e. the half-range Fourier Transform of  $f$ ) can be expressed in terms of the complete Fourier Transform  $\widehat{f}(z)$  and the Hilbert Transform  $\mathcal{H}[\widehat{f}(z)]$ :*

$$\widehat{f}_{\pm}(z) = \frac{1}{2} \{ \widehat{f}(z) \pm i\mathcal{H}[\widehat{f}(z)] \}, \quad (1.2)$$

known as Plemelj-Sokhotsky relations.

*Proof.* The aim is to find an expression for  $\widehat{f}_{+}(z) = \mathcal{F}_{x \rightarrow z}[f(x)\mathbb{1}_{\{x \geq 0\}}]$  and  $\widehat{f}_{-}(z) = \mathcal{F}_{x \rightarrow z}[f(x)\mathbb{1}_{\{x < 0\}}]$ , using the Hilbert Transform of  $\widehat{f}(z)$ . Following the approach of King (2009, pp. 252-261), considering that the inverse Fourier Transform:

$$\mathcal{F}_{z \rightarrow x}^{-1} \left[ \frac{1}{\pi z} \right] = -i \cdot \text{sgn}(x),$$

and then applying the convolution theorem  $\widehat{f}(z) * \widehat{g}(z) = \mathcal{F}[f(x)g(x)]$  to expression (1.1), we get:

$$\begin{aligned} \mathcal{H}[\widehat{f}(z)] &= \mathcal{F}_{x \rightarrow z}[-i \cdot \text{sgn}(x)f(x)] \\ i\mathcal{H}[\widehat{f}(z)] &= \mathcal{F}_{x \rightarrow z}[\text{sgn}(x)f(x)]. \end{aligned}$$

Finally, recalling that  $\text{sgn}(x)f(x) = f(x)\mathbb{1}_{x \geq 0} - f(x)\mathbb{1}_{x < 0}$  and by linearity of the integral, it's immediate that:

$$\begin{cases} \widehat{f}_{+}(z) - \widehat{f}_{-}(z) = i\mathcal{H}[\widehat{f}(z)] \\ \widehat{f}_{+}(z) + \widehat{f}_{-}(z) = \widehat{f}(z). \end{cases}$$

Thus, it's easy to recover the expressions in (1.2). ■

## 1.2.2 Laplace Transform and Z-Transform

In this section, we give the definition of Laplace Transform and its relation with its discrete version, the Z-transform, is studied. Indeed, this is a fundamental step that allows us to move from discrete to continuous time.

**Definition 1.4** (Laplace Transform). *The Laplace Transform of a function  $f(t)$  is an integral function defined as:*

$$\tilde{f}(s) = \mathcal{L}_{t \rightarrow s}[f(t)] = \int_0^{+\infty} f(t)e^{-st} dt, \quad \forall s \in \mathbb{C}.$$

The Inverse Laplace Transform can be expressed as (e.g. Arfken (1985)):

$$f(t) = \mathcal{L}_{s \rightarrow t}^{-1}[\tilde{f}(s)] = \frac{1}{2\pi i} \int_{a-i\infty}^{a+i\infty} e^{st} \tilde{f}(s) ds,$$

where  $s = a$  is a vertical contour in the Complex Plane chosen so that all singularities of  $\tilde{f}(s)$  are to the left of it.

**Definition 1.5** (Z-Transform). *The Z-Transform of a discrete function  $f$  that takes values on a grid of points with time step  $\Delta t$ , such that  $t_0 = 0$  and  $t_n = n\Delta t$ ,  $n \in \mathbb{N}$  is defined as:*

$$\mathcal{Z}_{n \rightarrow q}[f(t_n)] = \sum_{n=0}^{\infty} q^n f(t_n).$$

It's possible to connect Laplace transform and Z-Transform, as done in Phelan et al. (2018), considering the discretization of the integral in the Laplace Transform obtained introducing the grid  $t_n = n\Delta t$ :

$$\begin{aligned} \mathcal{L}_{t \rightarrow s}[f(t)] &= \int_0^{+\infty} e^{-st} f(t) dt = \lim_{\Delta t \rightarrow 0} \Delta t \sum_{n=0}^{\infty} e^{-sn\Delta t} f(n\Delta t) \\ &= \lim_{\Delta t \rightarrow 0} \Delta t \sum_{n=0}^{\infty} (e^{-s\Delta t})^n f(t_n) = \lim_{\Delta t \rightarrow 0} \Delta t \sum_{n=0}^{\infty} q^n f(t_n) \end{aligned}$$

Therefore:

$$\mathcal{L}_{t \rightarrow s}[f(t)] = \lim_{\Delta t \rightarrow 0} \Delta t \mathcal{Z}_{n \rightarrow q}[f(t_n)], \quad (1.3)$$

where  $q = e^{-s\Delta t}$ .

## 1.3 Wiener-Hopf Factorization and Spitzer Identity

The Wiener-Hopf method is a mathematical technique that solves the problem of decomposing a complex function  $\hat{f}$  into two functions  $\hat{f}_+$  and  $\hat{f}_-$  which are analytic in the upper and lower halves of the complex plane respectively. Moreover, we introduce the Spitzer Identity and its connection with the Wiener-Hopf factorization.

### 1.3.1 Wiener-Hopf Factorization

As explained in detail in Lawrie and Abrahams (2007), the Wiener-Hopf technique was initially proposed in order to solve for the unknown  $f$  the integral equation of the form:

$$\int_0^{\infty} k(x-y)f(y)dy = g(x), \quad x \in [0, \infty), \quad (1.4)$$

where  $k(x-y)$  and  $g(x)$  are known functions. The method starts with the extension of the right-hand side of the equation to the negative half of the real line to an unknown  $h$  and with the general definition of the half-range Fourier Transform:

$$\widehat{f}_+(z) = \int_0^{\infty} f(x)e^{ixz}dx, \quad \widehat{f}_-(z) = \int_{-\infty}^0 f(x)e^{ixz}dx.$$

With this elements, it is possible to rewrite the integral equation (1.4) in the Fourier domain as:

$$\widehat{f}_+(z)\widehat{k}(z) = \widehat{g}_+(z) + \widehat{h}_-(z).$$

The procedure relies on finding a product factorization:

$$\widehat{k}(z) = \widehat{k}_+(z)\widehat{k}_-(z),$$

where the subscript '+' ('-') represents a function analytic in the upper (respectively lower) complex plane with respect to a strip in which the function  $\widehat{k}(z)$  and both the ' $\pm$ ' factors are analytic. The sum decomposition of  $\widehat{g}$  and product factorizations of  $\widehat{k}$  can be found analytically, since  $g(x)$  and  $k(x)$  are known. It is possible to express (see Kisil (2015) for details) the factorization in terms of a Cauchy integral, instead of the Fourier Transform representation: indeed, this is the most used form in the definition of the Wiener-Hopf factors.

**Theorem 1.1** (Wiener-Hopf Factorization). *Let  $\widehat{f}(z)$  be a function of variable  $z = a + ib$  analytic in the strip  $b \in (b_-, b_+)$ , such that  $\widehat{f}(z) < C|a|^{-p}$ ,  $p > 0$  as  $|a| \rightarrow \infty$  uniformly  $\forall b$  in the strip. Then, for  $c, d \in (b_-, b_+)$ ,  $c \leq d$ :*

$$\widehat{f}(z) = \widehat{f}_+(z) + \widehat{f}_-(z),$$

$$\widehat{f}_+(z) = \frac{1}{2\pi i} \int_{-\infty+id}^{+\infty+id} \frac{\widehat{f}(u)}{u-z} du, \quad \widehat{f}_-(z) = -\frac{1}{2\pi i} \int_{-\infty+ic}^{+\infty+ic} \frac{\widehat{f}(u)}{u-z} du,$$

where  $\widehat{f}_-(z)$  is analytic in  $\Im(z) < b_+$  and  $\widehat{f}_+(z)$  is analytic in  $\Im(z) > b_-$  (e.g., see Th. 3.1 Kisil (2015, p. 1573)).

Taking the logarithm, one can get the product Wiener-Hopf Factorization:

**Theorem 1.2.** *If  $\widehat{f}(z) = \log(\widehat{k}(z))$  satisfies the conditions of Theorem 1.1, then  $\widehat{k}(z) = \widehat{k}_+(z)\widehat{k}_-(z)$ , where the factors are the exponential of the sum decomposition of  $\widehat{f}(z)$  (e.g., see Th. 6.1, 6.4 Kisil (2015, pp. 1576-1577)).*

In order to go back to the Fourier expression, we consider  $\widehat{f}(z)$  as the Fourier Transform of a certain function  $f$ , and take  $c = d = 0$ :

**Proposition 1.3.** *The Wiener-Hopf decomposition of the Fourier Transform  $\widehat{f}(z) = \mathcal{F}_{x \rightarrow z}[f(x)]$  is given by:*

$$\widehat{f}_+(z) = \mathcal{F}_{x \rightarrow z}[f(x)\mathbb{1}_{[0,+\infty)}(x)], \quad \widehat{f}_-(z) = \mathcal{F}_{x \rightarrow z}[f(x)\mathbb{1}_{(-\infty,0]}(x)].$$

*Proof.* (e.g. King (2009, pp. 111-113)) It's easy to prove the proposition given the definition of Wiener-Hopf factor. Here, only the case of  $\widehat{f}_+$  is explicitly shown; the procedure for  $\widehat{f}_-$  is similar.

$$\begin{aligned} \widehat{f}_+(z) &= \mathcal{F}_{x \rightarrow z}[f(x)\mathbb{1}_{[0,+\infty)}(x)] = \int_0^{+\infty} f(x)e^{izx} dx = \\ &= \frac{1}{2\pi} \int_0^{+\infty} e^{izx} \int_{-\infty}^{+\infty} \widehat{f}(u)e^{-iux} du dx. \end{aligned}$$

We then exchange the order of integration, since the Fourier Transform is  $L^2$ -integrable:

$$= \frac{1}{2\pi} \int_{-\infty}^{+\infty} \widehat{f}(u) \int_0^{+\infty} e^{i(z-u)x} dx du = \frac{1}{2\pi} \int_{-\infty}^{+\infty} \widehat{f}(u) \left[ \frac{e^{i(z-u)x}}{i(z-u)} \right]_0^{-\infty} du =$$

This quantity converges if and only if  $\Re(i(z-u)) < 0 \Rightarrow \Im(z) > 0$ , getting:

$$= \frac{1}{2\pi i} \int_{-\infty}^{+\infty} \frac{\widehat{f}(u)}{u-z} du, \quad \Im(z) > 0.$$

■

Therefore, it's possible to recover the Wiener-Hopf factorization through the Hilbert transform, thanks to its connection with the half-range Fourier transforms.

### 1.3.2 Spitzer Identity

In this paragraph a fundamental theorem will be introduced: the Spitzer Identity, proven in Spitzer (1956) through the use of combinatorial arguments. The formula connects the characteristic functions of a discrete random process with i.i.d. increments and the one of its maximum (or minimum). Moreover, it is shown the equivalence between the factorization implicit in the expression and the Wiener-Hopf one, introduced in the previous paragraph.

**Theorem 1.3** (Spitzer Identity). *Let  $\{X_n\}$  be a discrete random process where the increments  $\Delta X_n = X_n - X_{n-1}$  are a sequence of i.i.d random variables with  $X_0 = 0$ . Define  $\bar{X}_n = \max_{i=0,\dots,n} X_i$  and the notation  $f^\pm = (|f| \pm f)/2$ . Then:*

$$\sum_{n=0}^{\infty} q^n \mathbb{E}[e^{ia\bar{X}_n + ib(\bar{X}_n - X_n)}] = \exp \left\{ \sum_{n=1}^{\infty} \frac{q^n}{n} (\mathbb{E}[e^{iaX_n^+}] + \mathbb{E}[e^{ibX_n^-}] - 1) \right\},$$

with  $a, b \in \mathbb{R}$  (e.g. see Wendel (1958, p. 905)).

The identity states that it is possible to express the Z-Transform of the characteristic function of a linear combination of a discrete random process  $X_n$  with i.i.d increments and of its partial maximum  $\bar{X}_n$  as the exponential of a series involving the characteristic functions of the positive and negative part of  $X_n$ . Setting particular values for the parameters  $a$  and  $b$ , it's possible to obtain some interesting results that will be very useful for the continuation of our work.

- *Z-Transform of the characteristic function of the partial maximum  $\bar{X}_n$ :*  
Choosing  $a = z$  and  $b = 0$ , the equation becomes:

$$\begin{aligned} \sum_{n=0}^{\infty} q^n \mathbb{E}[e^{iz\bar{X}_n}] &= \exp \left\{ \sum_{n=1}^{\infty} \frac{q^n}{n} \mathbb{E}[e^{izX_n^+}] \right\} \\ &= \exp \left\{ \sum_{n=1}^{\infty} \frac{q^n}{n} \mathbb{E}[e^{izX_n}, X_n \geq 0] \right\} \exp \left\{ \sum_{n=1}^{\infty} \frac{q^n}{n} \mathbb{P}(X_n < 0) \right\}. \end{aligned} \quad (1.5)$$

- *Z-Transform of the characteristic function of  $X_n$ :*  
Choosing  $a = z$  and  $b = -z$ , the equation becomes:

$$\sum_{n=0}^{\infty} q^n \mathbb{E}[e^{izX_n}] = \exp \left\{ \sum_{n=1}^{\infty} \frac{q^n}{n} (\mathbb{E}[e^{izX_n^+}] + \mathbb{E}[e^{-izX_n^-}] - 1) \right\}.$$

Now let's consider only the expression in brackets on the right-hand side:

$$\begin{aligned} &\mathbb{E}[e^{izX_n^+}] + \mathbb{E}[e^{-izX_n^-}] - 1 = \\ &= \mathbb{E}[e^{izX_n}, X_n \geq 0] + \mathbb{P}(X_n < 0) + \mathbb{E}[e^{izX_n}, X_n < 0] + \mathbb{P}(X_n \geq 0) - 1 \\ &= \mathbb{E}[e^{izX_n}, X_n \geq 0] + \mathbb{E}[e^{izX_n}, X_n < 0], \end{aligned}$$

which will lead to the factorization of the Z-transform as:

$$\sum_{n=0}^{\infty} q^n \mathbb{E}[e^{izX_n}] = \underbrace{\exp \left\{ \sum_{n=1}^{\infty} \frac{q^n}{n} \mathbb{E}[e^{izX_n}, X_n \geq 0] \right\}}_{1/L_+(z,q)} \underbrace{\exp \left\{ \sum_{n=1}^{\infty} \frac{q^n}{n} \mathbb{E}[e^{izX_n}, X_n < 0] \right\}}_{1/L_-(z,q)}.$$

**Remark.** It's easy to see that we can rewrite the expression for the maximum in terms of  $L_{\pm}$ :

$$\sum_{n=0}^{\infty} q^n \mathbb{E}[e^{iz\bar{X}_n}] = \frac{1}{L_+(z, q)L_-(0, q)}.$$

Thus, thanks to the Spitzer identity, we saw how it is possible to factorize the Z-Transform of the characteristic function of a discrete random process with i.i.d increments. Moreover, it is possible to show that this factorization actually corresponds to the Wiener-Hopf product factorization. First, let's rewrite the expression for the Z-Transform of the characteristic function of  $X_n$  in a more convenient way:

$$\sum_{n=0}^{\infty} q^n \mathbb{E}[e^{izX_n}] = \sum_{n=0}^{\infty} q^n \mathbb{E}[e^{iz\sum_{k=1}^n \Delta X_k}] = \sum_{n=0}^{\infty} q^n \mathbb{E}[e^{iz\Delta X_1} \cdot \dots \cdot e^{iz\Delta X_n}]$$

Since all  $\Delta X_k$  are independent, the expected value of the product is the product of the expected values; moreover, they are all identically distributed  $\Delta X_k \sim Y \quad \forall k$ , therefore:

$$= \sum_{n=0}^{\infty} q^n (\mathbb{E}[e^{izY}])^n = \sum_{n=0}^{\infty} (q\mathbb{E}[e^{izY}])^n = \frac{1}{1 - q\mathbb{E}[e^{izY}]}, \quad (1.6)$$

given that the quantity  $|q\mathbb{E}[e^{izY}]| < 1$ .

**Proposition 1.4** (Spitzer and Wiener-Hopf connection). *The factorization of the Z-Transform of the characteristic function of a discrete random process  $X_n$  with i.i.d increments  $\Delta X_k \sim Y$  induced by the Spitzer identity is equal to its Wiener-Hopf product factorization, i.e.:*

$$L_{\pm}(z, q) = \exp \left\{ \pm \frac{1}{2\pi i} \int_{-\infty}^{+\infty} \frac{\log(1 - q\mathbb{E}[e^{iuY}])}{u - z} du \right\}, \quad \Im(z) \gtrless \Im(u).$$

*Proof.* (e.g see Sgarra et al. (2006, p. 10) and Green et al. (2010, p. 267)) The idea is to use the series expansion:

$$\sum_{n=1}^{\infty} \frac{t^n}{n} = -\log(1 - t), \quad |t| < 1,$$

and directly replace the series expansion in the definition of Wiener-Hopf factors. For  $L_+(z, q)$ :

$$\begin{aligned} & \exp \left\{ \frac{1}{2\pi i} \int_{-\infty}^{+\infty} \frac{\log(1 - q\mathbb{E}[e^{iuY}])}{u - z} du \right\}, \quad \Im(z) > \Im(u) \\ &= \exp \left\{ -\frac{1}{2\pi i} \int_{-\infty}^{+\infty} \sum_{n=1}^{\infty} \frac{q^n (\mathbb{E}[e^{iuY}])^n}{n(u - z)} du \right\}, \quad \Im(z) > \Im(u) \\ &= \exp \left\{ -\sum_{n=1}^{\infty} \frac{q^n}{n} \left( \frac{1}{2\pi i} \int_{-\infty}^{+\infty} \frac{(\mathbb{E}[e^{iuY}])^n}{u - z} du \right) \right\}, \quad \Im(z) > \Im(u) \\ &= \exp \left\{ -\sum_{n=1}^{\infty} \frac{q^n}{n} \left( \frac{1}{2\pi i} \int_{-\infty}^{+\infty} \frac{\mathbb{E}[e^{iuX_n}]}{u - z} du \right) \right\}, \quad \Im(z) > \Im(u) \end{aligned}$$

Notice that by definition 1.1 and proposition 1.3:

$$\mathbb{E}[e^{izX_n}, X_n \geq 0] = \frac{1}{2\pi i} \int_{-\infty}^{+\infty} \frac{\mathbb{E}[e^{iuX_n}]}{u - z} du, \quad \Im(z) > \Im(u),$$

Therefore:

$$\begin{aligned} &= \exp \left\{ -\sum_{n=1}^{\infty} \frac{q^n}{n} \left( \frac{1}{2\pi i} \int_{-\infty}^{+\infty} \frac{\mathbb{E}[e^{iuX_n}]}{u - z} du \right) \right\}, \quad \Im(z) > \Im(u) \\ &= \exp \left\{ -\sum_{n=1}^{\infty} \frac{q^n}{n} \mathbb{E}[e^{izX_n}, X_n \geq 0] \right\} = L_+(z, q). \end{aligned}$$

The procedure for  $L_-(z, q)$  is similar. ■

Even if the Spitzer Identity has been introduced in discrete time, Baxter and Donsker (1957) showed that it is possible to extend the identities to continuous time. Thanks to their work, we can then move from the Z-Transform to the Laplace Transform without losing of generality, as we will see in next section.

### 1.3.3 From Discrete to Continuous Time

In the previous paragraph, we explained a method that allows to retrieve the Z-Transform of the characteristic function of a general discrete random process with i.i.d. increments. However, since the aim of this work is to analyze the continuous case for a Lévy Process, we move from the discrete Z-Transform to the continuous Laplace Transform using equation (1.3) and the explicit expression of the characteristic function of a Lévy Process through its characteristic exponent, as suggested in Phelan et al. (2018).

Let's consider the discrete time grid  $t_k = k\Delta t$ ,  $t_0 = 0$  and  $t_n = t$ . A discrete Lévy process  $X_n$  is defined by its i.i.d increments  $\Delta X_k$ , for  $k = 1, \dots, n$ , that follows a Lévy distribution:

$$\mathbb{E}[e^{iz\Delta X_k}] = \mathbb{E}[e^{izY}] = \Psi(z, \Delta t) = e^{\psi(z)\Delta t}. \quad (1.7)$$

Combining this representation with the expression (1.6), the Z-Transform of the characteristic function of a discrete Lévy Process  $X_n$  may be expressed as:

$$\mathcal{Z}_{n \rightarrow q}[\Psi(z, t_n)] = \frac{1}{1 - q\mathbb{E}[e^{izY}]} = \frac{1}{1 - q\Psi(z, \Delta t)}.$$

Moreover, we know from equation (1.3), that:

$$\mathcal{L}_{t \rightarrow s}[\widehat{f}(z, t)] = \lim_{\Delta t \rightarrow 0} \Delta t \mathcal{Z}_{n \rightarrow q}[\widehat{f}(z, t_n)].$$

Therefore, the Laplace transform of a continuous Lévy Process  $X_t$  is equal to:

$$\begin{aligned} \mathcal{L}_{t \rightarrow s}[\Psi(z, t)] &= \lim_{\Delta t \rightarrow 0} \frac{\Delta t}{1 - q\Psi(z, \Delta t)} = \lim_{\Delta t \rightarrow 0} \frac{\Delta t}{1 - e^{-s\Delta t} e^{\psi(z)\Delta t}} = \\ &= \lim_{\Delta t \rightarrow 0} \frac{\Delta t}{1 - e^{-(s-\psi(z))\Delta t}} = \frac{1}{s - \psi(z)}. \end{aligned}$$

Thus, the quantity to be decomposed with the Wiener-Hopf Factorization becomes:

$$\mathcal{L}_{t \rightarrow s}[\Psi(z, t)] = \frac{1}{s - \psi(z)} = \frac{1}{l_+(z, s)l_-(z, s)}.$$

Indeed, a limit similar to the one for the Laplace transform holds for the Wiener-Hopf Factors (see Green et al. (2010)):

$$\lim_{\Delta t \rightarrow 0} \frac{L_{\pm}(z, q)}{\sqrt{\Delta t}} = l_{\pm}(z, s).$$

This is a very important result, since the limit of the function that must be decomposed in discrete time diverges:

$$\lim_{\Delta t \rightarrow 0} |\log(1 - q\Psi(z, \Delta t))| = +\infty.$$

Therefore the continuous decomposition can't be seen as a limit case of the discrete one: the function to be decomposed is different and it's given by the Laplace Transform.

**Remark.** Also the expression for the partial maximum can be moved to continuous time:

$$\mathcal{L}_{t \rightarrow s}[\Psi^M(z, t)] = \frac{1}{l_+(z, s)l_-(0, s)}. \quad (1.8)$$



## 1.4 Lewis-like method for Option Pricing

In this section we apply all the mathematical definitions seen up to now in order to get a pricing formula for exotic options with the approach followed both in Phelan et al. (2018) and Fusai et al. (2016). In those papers, the method refers to the original one introduced by Lewis (2001), which is well-known for plain vanilla options. It assumes that the asset evolves following an Exponential Lévy Process, thus the log-return follows a Lévy Process dynamics, for which the characteristic function is given in analytic form.

**Definition 1.6** (Log-return of an asset). *The log-return  $X_t$  of an asset  $S_t$  with initial value  $S_0$  at  $t = 0$  is defined as:*

$$X_t = \log \left( \frac{S_t}{S_0} \right).$$

Moreover, considering for an option a certain strike price  $K$ , let's introduce the log-strike  $k = \log \left( \frac{K}{S_0} \right)$ . The payoff of a plain vanilla call option is given by:

$$\phi(x) = (S_T - K)^+ = S_0(e^x - e^k) \mathbb{1}_{[k, +\infty)}(x).$$

Of course, similar expressions can be deduced also for a put option or digital options.

**Remark.** A digital option is a cash-or-nothing option, i.e. its payoff is 0 or 1 depending on the occurrence of a certain condition. In particular, a digital call option has payoff at maturity:

$$\phi^D(x) = \mathbb{1}_{[k, +\infty)}(x).$$

However, the call option payoff is not bounded and the Fourier transform of the payoff has poles in  $z = 0$  and  $z = -i$ : those elements are well-known as critical points in Lewis (2001). For that reason, Fusai et al. (2016) introduce the concept of damped payoff, also used in Carr and Madan (1999):

$$\phi_\gamma(x) = e^{\gamma x} S_0(e^x - e^k) \mathbb{1}_{[k, +\infty)}(x),$$

where the parameter  $\gamma$  ensures integrability of the payoff function. The choice of parameter  $\gamma$  has been deeply analyzed by Feng and Linetsky (2008), and we will study the effect of the choice of the damping parameter in the chapter 3.

The option present value is equal to the discounted payoff at  $t_0 = 0$ , given that we apply an appropriate risk-neutral probability distribution function  $p_T(x)$  for  $X_T$ ; in addition, we have the information  $X_0 = 0$ , therefore:

$$\begin{aligned} V(X_0, t_0) &= \mathbb{E}_0[V(x, T) | X_0 = 0] = e^{-rT} \int_{-\infty}^{+\infty} \phi(x) p_T(x) dx \\ &= e^{-rT} \int_{-\infty}^{+\infty} \phi_\gamma(x) e^{-\gamma x} p_T(x) dx. \end{aligned}$$

Then, applying the Plancherel relation to the integral and considering  $\widehat{\phi}_\gamma(z)$ , i.e. the Fourier Transform of the damped payoff, and  $\widehat{p}_T(z + i\gamma)$ , i.e. the Fourier Transform of the expression  $e^{-\gamma x} p_T(x)$ , we get:

$$V(X_0, t_0) = e^{-rT} \mathcal{F}_{z \rightarrow x}^{-1}[\widehat{\phi}_\gamma(z) \widehat{p}_T^*(z + i\gamma)](0) \quad (1.9)$$

$$= e^{-rT} \mathcal{F}_{z \rightarrow x}^{-1}[\widehat{\phi}_\gamma^*(z) \widehat{p}_T(z + i\gamma)](0). \quad (1.10)$$

where the  $\widehat{f}^*$  stands for the complex conjugate of  $\widehat{f}$ . Notice that (1.9) and (1.10) are interchangeable. The problem is to find the expressions for  $\widehat{\phi}_\gamma$  and  $\widehat{p}_T$ .

The first expression  $\widehat{\phi}_\gamma$  depends on the payoff we are studying and can be derived via analytical computations. For a call option, the Fourier Transform of the damped payoff can be found directly as:

$$\widehat{\phi}_\gamma(z) = \int_{-\infty}^{+\infty} e^{izx} \phi_\gamma(x) dx = S_0 \left[ \int_k^{+\infty} e^{(1+\gamma+iz)x} dx - e^k \int_k^{+\infty} e^{(\gamma+iz)x} dx \right],$$

where the two integrals converge for  $\gamma < -1$ ; finally, the expression needed is:

$$\widehat{\phi}_\gamma(z) = S_0 \frac{e^{(1+\gamma+iz)k}}{(\gamma+iz)(1+\gamma+iz)}.$$

For a digital call option, it is possible to obtain the Fourier transform of the damped payoff as:

$$\widehat{\phi}_\gamma^D(z) = -\frac{e^{(\gamma+iz)k}}{\gamma+iz}, \quad \gamma < 0.$$

The expression and the interval for  $\gamma$  in which the integral converges can be found in a similar way as for the call.

The second expression  $\widehat{p}_T$  is the damped characteristic function of the process  $X_T$ , that depends on the model for log-returns we are considering. Applying numerical techniques such as the Fast Fourier Transform (FFT) algorithm to the formulas (1.9) and (1.10), it's easy to price plain vanilla or digital options with different Lévy models for the dynamics of the log-returns, since the characteristic function of Lévy processes is known in closed form, as we saw in the first section of this work. The problem arises when pricing Exotic options such as lookback options or barrier options: in those cases, the options are path-dependent and we will need to know the distribution, in terms of characteristic function, of the extrema of the log-returns, i.e. of their maximum or minimum.

In this thesis, we study a single barrier down & out call option and a fixed strike lookback call option, providing also the method for their digital version. The models for log-returns considered in this work are in the family of the Lévy Processes, in particular the Brownian Motion, because it will allow us to compare the goodness of the new method with respect to the exact result of the closed formulas, and the NIG process.

### 1.4.1 Single Barrier Option

**Definition 1.7** (Barrier Option). *A Barrier Option is an option whose payoff at maturity depends on the fact that the underlying asset has touched or not a certain barrier during the lifetime of the option. Knock-out options cease to exist if the barrier is touched, while knock-in options activate if the underlying reaches the barrier level.*

In particular, we focus on a Single Barrier Down & Out Call Option, which has the payoff of a call option at maturity, given the fact that the asset has always been above a certain lower barrier  $B$  in  $[0, T]$ . In order to apply the method explained before, first we use the payoff expression for a call with lower barrier at maturity:

$$\phi(x) = S_0(e^x - e^k) \mathbb{1}_{[\max(k, b), \infty)}(x),$$

where  $b = \log(B/S_0)$  is the lower log-barrier. Plus, we should not consider as underlying process the log-return  $X_T$ , but the random process which is given by  $X_T$  with minimum  $\underline{X}_T$  always above the lower log-barrier  $b$ . In order to make things easier, let's start from the discrete case, following the approach of Green et al. (2010, pp. 262-264). Consider the transition probability from state  $x$  to state  $y$  for a discrete Lévy process  $X_k$ :

$$k(y - x)dy = \mathbb{P}(X_j \in [y, y + dy] | X_{j-1} = x),$$

where  $X_j$  is the process at time  $t_j = j\Delta t$ . Indeed, we know that a Lévy Process is a Markov process with stationary increments, therefore the definition above is coherent with our general framework. The probability density at step  $n$  for a process that has always been above a certain barrier  $b$  can be expressed as:

$$p_n^{(b)}(x) = \mathbb{P}(\{X_n \in [x, x + dx]\} \cap \{\underline{X}_{n-1} \geq b\}), \quad x \geq b$$

where  $\underline{X}_n = \min_{j=0, \dots, n} X_j$ , which recursively becomes:

$$\begin{cases} p_n^{(b)}(y) = \int_b^\infty p_{n-1}^{(b)}(x)k(y-x)dx, \\ p_0^{(b)}(y) = \delta(y). \end{cases} \quad (1.11)$$

The idea is to recover an integral equation of the Wiener-Hopf form in order to apply the method to get the solution, i.e. the requested distribution function. First, let's introduce the Z-Transform of  $p_n^{(b)}(y)$ :

$$f(y, q) = \sum_{n=0}^{\infty} q^n p_n^{(b)}(y).$$

The following equation is then straightforward, applying the Z-Transform to (1.11):

$$f(y, q) - \delta(y) = q \int_b^\infty f(x, q)k(y-x)dx; \quad (1.12)$$

then we apply the change of variable  $\xi = y - b$ ,  $\nu = x - b$  and define  $g(\cdot) = f(\cdot + b, q)$ , so that we can apply the Wiener-Hopf method involving Fourier and half-range Fourier transform, with the integral in the right-hand side of the equation on  $[0, \infty)$ :

$$\begin{aligned} g(\xi) - \delta(\xi + b) &= q \int_0^\infty g(\nu)k(\xi - \nu)d\nu \\ \implies \widehat{g}(z) - e^{-izb} &= q(\widehat{g}_+(z)\widehat{k}(z)), \end{aligned}$$

where  $\widehat{k}(z) = \Psi(x, \Delta t)$  is the characteristic function of the original Lévy increment, while  $\widehat{g}_+(z) = \int_0^\infty g(x)e^{izx}dx$  and  $\widehat{g}_-(z) = \int_{-\infty}^0 g(x)e^{izx}dx$  are the

half-range Fourier transform of the shifted Z-Transform of  $p_n^{(b)}(y)$ .

Rearranging the terms of the equation and calling  $L(z) = 1 - q\Psi(z, \Delta t)$ , we get:

$$\widehat{g}_+(z)L(z) = e^{-izb} - \widehat{g}_-(z),$$

which is a Wiener-Hopf problem with unknown  $g(z)$ . Moreover, notice that  $L(z)$  is the denominator of the Z-Transform of the characteristic function of the process  $X_n$ , as derived according to the Spitzer Identity at equation (1.6). In addition, the function we are interested in is the characteristic function for the process above the barrier  $b$ ; writing down explicitly  $f(x) = \sum_{n=0}^{\infty} q^n p_n^{(b)}(x)$  with  $\widehat{g}_{\pm}$ :

$$f(x) = \begin{cases} \mathcal{F}_{z \rightarrow x}^{-1}[e^{izb}\widehat{g}_+(z)], & x \geq b \\ \mathcal{F}_{z \rightarrow x}^{-1}[e^{izb}\widehat{g}_-(z)], & x < b, \end{cases}$$

therefore, since we are interested in the case  $x \geq b$ , we only need to compute  $\widehat{g}_+(z)$ . Following the Wiener-Hopf procedure explained in Kisil (2015), using the factorizations of  $L(z) = L_+(z)L_-(z)$  and  $J(z) = J_+(z) + J_-(z)$  with  $J(z) = e^{-izb}/L_-(z)$ , the equation becomes:

$$\widehat{g}_+(z)L_+(z) - J_+(z) = J_-(z) - \frac{\widehat{g}_-(z)}{L_-(z)}.$$

The expression above equates a left term which is analytic in and above the analytic region for  $L(z)$  and a right term analytic in and below the same region: assuming  $g(\cdot)$  bounded at 0, it is possible to apply Liouville's theorem, and therefore both members should be constant and equal to 0. Therefore:

$$\widehat{g}_+(z) = \frac{J_+(z)}{L_+(z)},$$

where  $J_+(z)$  and  $L_+(z)$  are the Wiener-Hopf factors with integral Cauchy representation:

$$L_+(z) = \exp \left\{ \frac{1}{2\pi i} \int_{-\infty}^{+\infty} \frac{\log(L(u))}{u-z} du \right\}, \quad \Im(z) > \Im(u);$$

$$J_+(z) = \frac{1}{2\pi i} \int_{-\infty}^{+\infty} \frac{e^{-iub}}{L_-(u)(u-z)} du, \quad \Im(z) > \Im(u).$$

Moving to continuous time thanks to the paper of Baxter and Donsker (1957) as we did in section 1.3.3, we are therefore able to compute the Laplace Transform of the Characteristic function for the Lévy process with continuous barrier:

$$\widetilde{p}_s^{(b)}(z) = \frac{j_{b+}(z, s)}{l_+(z, s)},$$

where for  $l(z, s) = s - \psi(z)$ , with  $\psi(z)$  characteristic exponent, while  $j(z, s) = 1/l_-(z, s)$  is decomposed on the barrier  $b$ . The formula for the evaluation of a continuously monitored Down & Out Call Barrier Option is given by:

$$V^{D\&O}(X_0, t_0) = e^{-rT} \mathcal{F}_{z \rightarrow x}^{-1} \left[ \widehat{\phi}_\gamma^*(z) \mathcal{L}_{s \rightarrow T}^{-1} \left[ \frac{j_{b+}(z + i\gamma, s)}{l_+(z + i\gamma, s)} \right] \right] (0).$$

In order to compute  $\widetilde{p}_s^{(b)}(z + i\gamma)$ , one should:

1. first, compute  $h(z + i\gamma, s) = \log(l(z + i\gamma, s)) = \log(s - \psi(z + i\gamma))$ ;
2. then the Wiener-Hopf factors can be found using the relation between the Wiener-Hopf factorization and the Hilbert Transform:

$$h_{\pm}(z + i\gamma, s) = \frac{1}{2}(h(z + i\gamma, s) \pm i\mathcal{H}[h(z + i\gamma, s)]);$$

3. compute the product factors  $l_{\pm}(z + i\gamma, s) = e^{h_{\pm}(z + i\gamma, s)}$ ;
4. compute  $j(z + i\gamma, s) = 1/l_{-}(z + i\gamma, s)$  and decompose it with the Plemelj-Sokhotsky relations for a generalized barrier  $b$ :

$$j_{b\pm}(z, s) = \frac{1}{2}(j(z, s) \pm e^{izb}i\mathcal{H}[e^{-izb}j(z, s)])$$

### 1.4.2 Lookback Option

**Definition 1.8** (Lookback Option). *Given an underlying asset modelled with the process  $S_t$ , define the processes of the maximum and of the minimum:*

$$\bar{S}_T := \max_{t \in [0, T]} S_t \quad \text{and} \quad \underline{S}_T := \min_{t \in [0, T]} S_t;$$

Then, the Lookback Options are defined by their payoff at maturity  $t = T$ :

- *Floating Strike Call:*  $V_{fl}^{LC}(T) = S_T - \underline{S}_T$ ;
- *Floating Strike Put:*  $V_{fl}^{LP}(T) = \bar{S}_T - S_T$ ;
- *Fixed Strike (K) Call:*  $V_{fix}^{LC}(T) = (\bar{S}_T - K)^+$ ;
- *Fixed Strike (K) Put:*  $V_{fix}^{LP}(T) = (K - \underline{S}_T)^+$ .

In particular, we will consider the Fixed Strike Lookback Call Option. Let's rewrite the payoff in a more suitable way. First, it's immediate that:

$$\bar{S}_T = \max_{t \in [0, T]} S_t = \max_{t \in [0, T]} S_0 e^{X_t} = S_0 e^{\max_{t \in [0, T]} X_t} = S_0 e^{\bar{X}_T},$$

where  $\bar{X}_T = \max_{t \in [0, T]} X_t$  is the maximum of the log-returns, and also  $\bar{X}_T = \log(\bar{S}_T/S_0)$ ,  $\bar{X}_0 = X_0 = 0$ . Therefore, the payoff function for the fixed strike lookback call option at maturity is given by:

$$\phi(\bar{x}) = S_0(e^{\bar{x}} - e^k) \mathbb{1}_{[k, +\infty)}(\bar{x}),$$

which is basically the same of a plain vanilla call option, but with the difference that the variable  $\bar{x}$  is not directly the log-return, but it's maximum.

The idea is to apply the formula (1.10) using  $\widehat{p}_T^M(z)$ , the characteristic function of the maximum, instead of  $\widehat{p}_T(z)$ , the characteristic function of the log-returns. The method applied in order to find the needed characteristic function follows the steps of Fusai et al. (2016) and Green et al. (2010), but moving from

discrete time to continuous time monitored options. Even if it is not possible to find an analytic expression for the characteristic function of the maximum of a generic Lévy process  $\widehat{p}_t^M(z) = \Psi^M(z, t)$ , we saw in section 1.3.3 that it's possible to find its Laplace Transform as in expression (1.8):

$$\widetilde{p}_s^M(z) = \mathcal{L}_{t \rightarrow s}[\Psi^M(z, t)] = \frac{1}{l_+(z, s)l_-(0, s)},$$

where  $l_{\pm}(z, s)$  are the Wiener-Hopf factors of  $l(z, s) = s - \psi(z)$ . Therefore, the expression for the evaluation of the Fixed Strike Lookback Call Option is given by:

$$V_{fix}^{LC}(\bar{X}_0, t_0) = e^{-rT} \mathcal{F}_{z \rightarrow y}^{-1} \left[ \widehat{\phi}_{\gamma}^*(z) \mathcal{L}_{s \rightarrow T}^{-1} \left[ \frac{1}{l_+(z + i\gamma, s)l_-(0, s)} \right] \right] (0)$$

The steps needed in order to get the Laplace transform of the characteristic function of the maximum of the log-returns  $\widetilde{p}_s^M(z)$  are the following:

1. first, proceed as in points 1, 2 and 3 for the single barrier option, in order to find  $l_{\pm}(z + i\gamma, s)$ .
2. after that, compute the value of the '-' function in  $(0, s)$ ;
3. compute the required  $l_+(z + i\gamma, s)l_-(0, s) = e^{h_+(z+i\gamma, s)+h_-(0, s)}$ .

As one can notice, the pricing formulas for both single barrier options and lookback options imply at least three levels of integration and they can not be further simplified: the numerical methods used in order to deal with the inverse Fourier transform, the inverse Laplace transform and the computation of the Hilbert transform will be discussed in chapter 2.

### 1.4.3 Digital Options

In this framework, it is also possible to price digital options on the described processes. A digital call option with single lower barrier can be interpreted as a usual digital call with strike  $K$ , that vanishes if an American barrier  $B$  is touched (with  $K > B$ ). More interesting is a digital lookback call, which is basically an American digital option, i.e. it pays 1 if the price of the underlying asset is above the strike  $K$  at least once in the lifetime of the option. The pricing method is basically the same as the two options above: the only difference is in the damped payoff function's Fourier Transform to be considered.

## 1.5 Closed Formulas

Assuming a Brownian Motion model for the log-returns, and therefore a Geometric Brownian Motion model for the underlying asset, it's possible to derive analytically the distribution of the maximum. For that reason, it's also possible to write the analytical Black & Scholes-like formula for the price of the lookback and the single barrier options and their digital versions. Thanks to that, we can use the exact value of the closed formula as a reference value, and therefore study the order of convergence of the error of the analytical method. Therefore, in the remaining part of the chapter we report these closed formulas.

## Single Barrier Down & Out Call

For the Single Barrier Down & Out Call, the price of the option is computed in a different way if the barrier  $B$  is greater or smaller than the strike price  $K$ .

**Proposition 1.5.** *Consider a Black & Scholes framework in presence of dividend yields, with an underlying asset with dynamics under the risk-free neutral measure:*

$$dS_t = (r - q)S_t dt + \sigma S_t dW_t, \quad (1.13)$$

with initial asset price  $S_0$ , risk-free interest rate  $r$ , dividend yield  $q$ , volatility  $\sigma$  and Brownian Motion  $W_t$ . Introduce the plain vanilla call price  $C(S)$  with strike  $K$  as a function of the spot price  $S$ :

$$C(S) = S e^{-qT} \mathcal{N}(d_1) - K e^{-rT} \mathcal{N}(d_2),$$

$$d_1 = \frac{\log(S/K) + (r - q + \sigma^2/2)T}{\sigma\sqrt{T}}, \quad d_2 = d_1 - \sigma\sqrt{T}.$$

Then, the price of a Down & Out Call Option with barrier  $B$  with  $S_0 > B$  is equal to:

If  $B \leq K$ :

$$V_C^{D\&O}(0) = C(S_0) - \left(\frac{B}{S_0}\right)^{\frac{2r}{\sigma^2}-1} C\left(\frac{B^2}{S_0}\right).$$

If  $B \geq K$ :

$$V_C^{D\&O}(0) = S_0 e^{-qT} \left( \mathcal{N}(x_1) - \left(\frac{B}{S_0}\right)^{2\lambda} \mathcal{N}(y_1) \right) - K e^{-rT} \left( \mathcal{N}(x_2) - \left(\frac{B}{S_0}\right)^{2\lambda-2} \mathcal{N}(y_2) \right),$$

where  $\lambda = \frac{r-q}{\sigma^2} + \frac{1}{2}$  and:

$$x_1 = \frac{\log(S_0/B)}{\sigma\sqrt{T}} + \lambda\sigma\sqrt{T}, \quad x_2 = x_1 - \sigma\sqrt{T};$$

$$y_1 = \frac{\log(B/S_0)}{\sigma\sqrt{T}} + \lambda\sigma\sqrt{T}, \quad y_2 = y_1 - \sigma\sqrt{T}.$$

## Digital with Barrier

Similarly, the Black & Scholes formula for a digital call option with lower barrier and  $K \geq B$  is given by:

$$V_D^{D\&0} = \text{Dig}(S_0) - \left(\frac{B}{S_0}\right)^{\frac{2r}{\sigma^2}-1} \text{Dig}\left(\frac{B^2}{S_0}\right),$$

where  $\text{Dig}(S) = e^{-rT} \mathcal{N}(d_2)$  with  $d_2$  as in the call definition.

## Fixed Strike Lookback Call

In this work, we focus the analysis on a Lookback Call Option with fixed strike, for which the closed formula is given by the following expression:

**Proposition 1.6.** *Consider the same framework as proposition 1.5, with dynamics for  $S_t$  as in equation (1.13). Then, the price of a Lookback Call Option with Fixed Strike is equal to:*

If  $S_0 < K$ :

$$V_{fix}^{LC}(0) = S_0 e^{-qT} \mathcal{N}(d_1) - K e^{-rT} \mathcal{N}(d_2) + S_0 e^{-rT} \frac{\sigma^2}{2(r-q)} \left( - \left( \frac{S_0}{K} \right)^{-\frac{2(r-q)}{\sigma^2}} \mathcal{N}\left(d_1 - \frac{2(r-q)\sqrt{T}}{\sigma}\right) + e^{(r-q)T} \mathcal{N}(d_1) \right),$$

where

$$d_1 = \frac{\log(S_0/K) + (r-q + \sigma^2/2)T}{\sigma\sqrt{T}}, \quad d_2 = d_1 - \sigma\sqrt{T};$$

If  $S_0 \geq K$ :

$$V_{fix}^{LC}(0) = (S_0 - K)e^{-rT} + S_0(e^{-qT} \mathcal{N}(d_1) - e^{-rT} \mathcal{N}(d_2)) + S_0 e^{-rT} \frac{\sigma^2}{2(r-q)} \left( \mathcal{N}\left(d_1 - \frac{2(r-q)\sqrt{T}}{\sigma}\right) + e^{(r-q)T} \mathcal{N}(d_1) \right),$$

where

$$d_1 = \frac{(r-q + \sigma^2/2)T}{\sigma\sqrt{T}}, \quad d_2 = d_1 - \sigma\sqrt{T}.$$

## American Digital

In case of continuously monitored digital, let's consider that if we start with  $S_0 \geq K$ , we will receive 1 for sure, since we are already above the strike, then the option price is just the discount factor  $V_{fix}^{LD} = e^{-rT}$ ; otherwise, i.e. if  $S_0 < K$ , we have:

$$V_{fix}^{LD} = e^{-rT} \left( \mathcal{N}(d_2) + \left( \frac{K}{S_0} \right)^{\frac{2(r-q)}{\sigma^2} - 1} \mathcal{N}(d_3) \right),$$

where

$$d_2 = \frac{\log(S_0/K) + (r-q - \sigma^2/2)T}{\sigma\sqrt{T}}, \quad d_3 = \frac{\log(S_0/K) - (r-q - \sigma^2/2)T}{\sigma\sqrt{T}}.$$



## Chapter 2

# Numerical Methods

As mentioned before, the pricing formulas introduced in the previous chapter can't be solved in an analytic way, since they involve multiple levels of integration (Wiener-Hopf Factorization, Inverse Laplace Transform and Inverse Fourier Transform). For that reason, in this chapter we point out some numerical techniques which can be used in order to compute numerically the integrals, and therefore actually price the exotic options with the Wiener-Hopf method. While describing the numerical methods, we also discuss about their theoretical convergence and we introduce some test functions. Following the work of Phelan et al. (2018), we use the FFT algorithm for the Inverse Fourier Transform; about the computation of the Hilbert Transform, we expose the Sinc expansion technique, already used by Feng and Linetsky (2008) and first introduced by Stenger and McArthur (1994); finally, we exploit the trapezoidal rule with Euler acceleration for the computation of the Inverse Laplace Transform as shown in Abate and Whitt (1995).

### 2.1 FFT Procedure

The FFT algorithm is well-known: it is based on the Discrete Fourier Transform, but with the constraint that the number of points considered in the grid is a power of 2. In this way, it's possible to accelerate the computation of the discrete integral from  $\mathcal{O}(N^2)$  to  $\mathcal{O}(N \log(N))$ . In this work, this numerical technique is exploited in order to compute the Inverse Fourier Transform in formulas (1.9) and (1.10). The computation of the integral through a discretization implies to rely on a grid: this grid affects also the computation of the Hilbert Transform, used for the Wiener-Hopf factorization, since one can notice that the Hilbert Transform does not move the domain of the function, therefore we consider the same grid.

In this section, we will briefly show the application of the numerical scheme to our case, in order to identify the correct grid and the functions exploited in Matlab. For the sake of brevity, let's define the quantity to which the FFT algorithm should be applied as:

$$f(z) = \widehat{\phi}_\gamma^*(z) \mathcal{L}_{s \rightarrow T}^{-1} [\widetilde{p}_s(z + i\gamma)].$$

The expression in equation (1.10) can be rewritten as:

$$V(x_0, t_0) = e^{-rT} \mathcal{F}_{z \rightarrow x}^{-1}[f(z)] \Big|_{x=x_0} = \frac{e^{-rT}}{2\pi} \underbrace{\int_{-\infty}^{+\infty} e^{-izx_0} f(z) dz}_{I(x_0)},$$

thus the integral to be computed via FFT is:

$$I(x_0) = \int_{-\infty}^{+\infty} e^{-izx_0} f(z) dz \xrightarrow{\text{Discrete}} I(x_0) \approx \sum_{j=1}^N e^{ix_0 z_j} f(z_j) \Delta z.$$

The Matlab function `fft` takes a vector of points  $f_j$ , which are values on the grid of  $z$ , and transforms them in points  $FFT_l$  on the domain of  $x$  through the formula:

$$FFT_l = \sum_{j=1}^N e^{-\frac{2\pi i}{N}(l-1)(j-1)} f_j.$$

In order to obtain the integral we want to compute, we should define the grid in the following way:

$$x_l = x_1 + (l-1)\Delta x, \quad z_j = z_1 + (j-1)\Delta z,$$

with the constraint:

$$\Delta x \Delta z = \frac{2\pi}{N},$$

where  $N$  is a power of 2; therefore:

$$x_l z_j = x_l z_1 + x_1(j-1)\Delta z + (l-1)(j-1)\Delta z \Delta x.$$

With the FFT method, we can compute the value of the integral  $I(x)$  for all points  $x_l, \forall l = 1, \dots, N$ :

$$I(x_l) = \sum_{j=1}^N e^{ix_l z_j} f(z_j) \Delta z = e^{-ix_l z_1} \sum_{j=1}^N e^{-i(x_l - x_1)(j-1)\Delta z} (e^{-ix_1(j-1)\Delta z} f(z_j)) \Delta z.$$

Applying the Matlab function to  $f_j = e^{-ix_1(j-1)\Delta z} f(z_j)$ , then we get:

$$I(x_l) = e^{-ix_l z_1} FFT_l \Delta z. \quad (2.1)$$

We can notice that the two grids are connected: once chosen the step size  $\Delta z$  (or  $\Delta x$ ), both the grids are defined. Moreover, the points on the grids are symmetrical with respect to 0, i.e.  $z_1 = -z_N$  and  $x_1 = -x_N$ , which means that the grids are:

$$\begin{cases} x = -\frac{N-1}{2}\Delta x, \dots, +\frac{N-1}{2}\Delta x \\ z = -\frac{N-1}{2}\Delta z, \dots, +\frac{N-1}{2}\Delta z \end{cases}.$$

The option price is gained for  $x = x_0 = 0$ , therefore the value we are looking for is:

$$V(0, t_0) \approx \frac{e^{-rT}}{2\pi} I(0).$$

Because of symmetry, the value  $x = 0$  is not part of the grid: a simple `spline` interpolation will allow to get the required  $I(0)$ .

## 2.2 Sinc Expansion for Hilbert Transform

Numerically, the Hilbert Transform could be computed applying a double Fourier Transform, as we saw in section 1.2.1:

$$\mathcal{H}[\widehat{f}(z)] = -i\mathcal{F}_{x \rightarrow z}[\text{sgn}(x)\mathcal{F}_{z \rightarrow x}^{-1}[\widehat{f}(z)]].$$

However this is not the best approach, since it implies an error that decreases quadratically with the grid step size  $\Delta z$  (see Phelan et al. (2018)). Moreover, the Hilbert Transform doesn't change the domain from the real ( $x$ ) to the frequency one ( $z$ ) as the Fourier Transform does: it's a transformation applied in the same domain. In order to gain exponential error convergence, it is possible to introduce a different method proposed by Feng and Linetsky (2008) that relies on the work of Stenger and McArthur (1994) on the Sinc Expansion, exploiting the optimized matrix-vector multiplication in Matlab. Sinc methods are based on the use of the Sinc Function:

$$\text{sinc}(x) = \frac{\sin(\pi x)}{\pi x}, \quad \forall x \in \mathbb{R}.$$

Applying this function on a discretized grid, for certain particular functions it is possible to get an exact expansion, as in the theorem below:

**Theorem 2.1** (Sinc Expansion). *Let  $\Delta > 0$  and let  $W(\frac{\pi}{\Delta})$  the space of  $f$  analytic functions on  $\mathbb{C}$  such that  $\int_{\mathbb{R}} |f(x)|^2 dx < \infty$  and  $|f(z)| \leq Ce^{\frac{\pi}{\Delta}|z|}$  for some constant  $C$ . Then,  $\forall f \in W(\frac{\pi}{\Delta})$  it's possible to define the following exact Sinc Expansion:*

$$C(f, \Delta)(x) = \sum_{k=-\infty}^{+\infty} f(k\Delta) \text{sinc}\left\{\frac{x}{\Delta} - k\right\}, \quad \forall x \in \mathbb{R}.$$

(e.g. see Th. 6.1, Feng and Linetsky (2008)).

If the function is not analytic on the whole complex plane, the expansion is no more exact, but if  $f$  still satisfies the other hypothesis, then it becomes an approximation. In particular:

**Proposition 2.1.** *If  $f$  is analytic in a strip of the complex plane, i.e.  $\mathcal{D}_d = \{z \in \mathbb{C} : |\Im(z)| < d\}$ , then the approximation error induced by the series is exponentially bounded:*

$$\sup_{x \in \mathbb{R}} |f(x) - C(f, \Delta)(x)| = \mathcal{O}(e^{-\frac{\pi}{\Delta}d}), \quad \text{for } \Delta \rightarrow 0.$$

(e.g. see Stenger (2000, p. 383)).

Let's consider the function on which we are going to apply the expansion:

$$h(z, s) = \log(l(z, s)) = \log(s - \psi(z));$$

since we are considering a logarithm, the function is not analytic on the whole complex plane; however, it's possible to find a strip  $\{z : |\Im(z)| < d\}$  in which

the function is analytic, as we will numerically confirm in section 3.3. The Sinc expansion approximation of  $h(z, s)$  is given by:

$$h(z, s) \approx \sum_{k=-\infty}^{+\infty} h(k\Delta, s) \frac{\sin(\pi(z - k\Delta)/\Delta)}{\pi(z - k\Delta)/\Delta}. \quad (2.2)$$

In Stenger and McArthur (1994), the expansion of the function is also applied to get the Hilbert Transform, exploiting the known analytical form of the Hilbert transform for the Sinc function:

$$\mathcal{H}\left[\frac{\sin(x)}{x}\right] = \frac{1 - \cos(x)}{x}. \quad (2.3)$$

For that reason, it's easy to get the approximation formula for the Hilbert Transform applying the relation (2.3) to (2.2) :

$$\mathcal{H}[h(z, s)] \approx \sum_{k=-\infty}^{+\infty} h(k\Delta, s) \frac{1 - \cos(\pi(z - k\Delta)/\Delta)}{\pi(z - k\Delta)/\Delta}, \quad \forall z \in \mathbb{R}.$$

Thus, we will have a discretization error which exponentially decays according to proposition (2.1). In addition, the infinite summation should also be truncated according to the grid size. As discussed, the grid for the computation of the Hilbert Transform is the same as the one used for the FFT, therefore the points of the discretization are explicitly:

$$z = -\frac{N-1}{2}\Delta z, \dots, +\frac{N-1}{2}\Delta z,$$

Calling  $\tilde{N} = \frac{N-1}{2}$  and  $\Delta z = \Delta$ , the final formula for the Hilbert Transform of  $h(z, s)$  will be:

$$\mathcal{H}[h(z, s)] \approx \sum_{k=-\tilde{N}}^{\tilde{N}} h(k\Delta z, s) \frac{1 - \cos(\pi(z - k\Delta z)/\Delta z)}{\pi(z - k\Delta z)/\Delta z}, \quad \forall z \in \mathbb{R}. \quad (2.4)$$

Of course, the truncation of the sum introduces a truncation error in addition to the approximation error. In particular, this error is exponentially bounded if the function  $h(z, s)$  decays at least exponentially as  $|z| \rightarrow \infty$ , otherwise this bound is no longer achieved. (e.g. see Phelan et al. (2017, p. 11)).

### 2.2.1 Toeplitz Matrix

Since the Hilbert Transform is computed on a grid, that we have seen is the same grid used in the FFT algorithm, the computation of the Hilbert Transform can be reduced to a matrix-vector multiplication. Indeed, when computing the Hilbert transform for each point on the grid  $z_j = j\Delta z$ ,  $j = -\tilde{N}, \dots, \tilde{N}$ , the cosine series in the formula (2.4) actually depends only on the number of grid steps between  $z_j$  and all the other grid points, i.e. the quantity:

$$\frac{1 - \cos(\pi(z_j - k\Delta z)/\Delta z)}{\pi(z_j - k\Delta z)/\Delta z} = \frac{1 - \cos(\pi(j - k))}{\pi(j - k)} = \begin{cases} 0, & \text{if } j-k \text{ is even,} \\ \frac{2}{j-k}, & \text{if } j-k \text{ is odd.} \end{cases}$$

Moreover, it is known that the limit:

$$\lim_{x \rightarrow 0} \frac{1 - \cos(x)}{x} = 0,$$

which can be used when evaluating the quantity for  $j = k$ . Therefore, if we define a  $N \times N$ -matrix  $\mathbf{T}$ :

$$T_{j,k} = \begin{cases} 0, & \text{if } j-k \text{ is even or } 0, \\ \frac{2}{j-k}, & \text{if } j-k \text{ is odd,} \end{cases}$$

and if we consider the column vector  $\mathbf{h}$  as a  $N$ -vector given by the evaluation of  $h(z, s)$  on the grid points  $z_j = j\Delta z$ ,  $j = -\tilde{N}, \dots, \tilde{N}$ , the column vector  $\mathbf{H}$  with the values of the Hilbert Transform on the same grid points can be computed as:

$$\mathbf{H} = \mathbf{T}\mathbf{h}.$$

In particular, notice that  $\mathbf{T}$  is a Toeplitz matrix, i.e. is constant on the diagonals, having  $T_{j,k} = T_{j+1,k+1}$ . For that reason, the matrix is completely defined by its first row and first column. It is possible to exploit some Matlab functions in the package `toeplitz` in order to speed up the matrix-vector multiplication and avoid to store the whole matrix. In this way, it is possible to expand the grid up to  $N = 2^{16}$  points.

## 2.2.2 Exponential Filter

In order to improve convergence, the work of Phelan et al. (2017) suggests the use of a filter, that may be multiplied to the input of the Hilbert transform. This procedure has been used also in order to improve the convergence of the Discrete Fourier Transform method in case of functions that are affected by the Gibbs Phenomenon, as studied in Gottlieb and Shu (1997). In this paper, it's described how it's possible to use a filter in case of series expansion of a function, as in our case. We will use an exponential filter, as defined in Gottlieb and Shu (1997).

**Definition 2.1** (Exponential filter of order  $p$ ). *A filter of order  $p$  is defined as a function  $\sigma(\eta)$  supported on  $\eta \in [-1, 1]$  with the properties:*

- $\sigma(0) = 1, \sigma^{(l)}(0) = 0$ ;
- $\sigma(\eta) = 0$  for  $|\eta| = 1$ ;
- $\sigma(\eta) \in C^{p-1}$ .

*In particular, the exponential filter of order  $p$  has form:*

$$\sigma(\eta) = e^{-\theta|\eta|^p},$$

*where  $p$  is even.  $\theta$  and  $\eta$  depends on the application.*

In our case, following the approach of Phelan et al. (2018), we choose  $\theta < \epsilon \log(10)$ , where  $10^{-\epsilon}$  is the machine precision, therefore we select  $\theta = 16 \log(10)$ . Then, since the filter has support on  $\eta \in [-1, 1]$ , we consider  $\eta = z/z_{max}$ . The filter has different shapes for different values of  $p$ : with small  $p$ , the effect of the filter is visible on a wider range of  $\eta$ , while increasing  $p$  the effect is more on the tail, as it's possible to see in figure 2.1 (c.f. Fig. 1, Phelan et al. (2018, p. 214)).

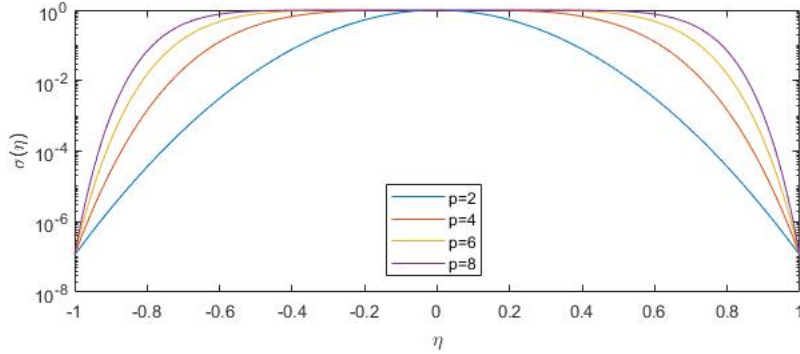


Figure 2.1: Exponential filter for different values of  $p$ .

### 2.2.3 Numerical Tests

We perform some numerical tests in order to study possible effects of the filter on the error convergence: we consider three different functions for which the analytic form of the Hilbert transform is known. For each case, first we should select a reasonable value for the parameter  $p$ ; then, we can proceed on comparing the convergence of the error with or without the filter with respect to the number of points of the grid  $N$ . Each function has different features, so that we can verify the behaviour of the method in different cases.

- a. The simplest case is the Cauchy function, which is an analytic function with well-behaving tails (no asymptotic) and with no discontinuities:

$$f(x) = \frac{1}{x^2 + 1} \xrightarrow{\text{Hilbert}} \mathcal{H}[f(x)] = \frac{x}{x^2 + 1}.$$

We don't expect the filter to have a great impact in this case, since the function is a regular one. Indeed, as we can see in figure 2.2, the filter runs out of its effect with small values of  $p$ , since after  $p = 12$  we don't have a visible improving. Moreover, thanks to the regularity of the function, the method applied to compute the Hilbert Transform has already a convergent error, therefore the filter has the only effect to slightly increase the convergence in  $N$ .

- b. In order to apply the method to an oscillating function both on the real and on the imaginary part of the spectrum, we use:

$$f(x) = e^{ix} \xrightarrow{\text{Hilbert}} \mathcal{H}[f(x)] = -i\text{sgn}(x)e^{ix}.$$

In this case we would like to study the effect of the filter on the central part of the approximation, since we know that for sure the tails will be affected by the correction and therefore they will no more show an oscillating shape, as we can see in figure 2.3.

After that, we select  $p$  as before: looking at the first plot of figure 2.4 it's clear that here the filter has much more effect, since we see an increasing in precision up to  $p = 50$ . The convergence of the absolute errors both in

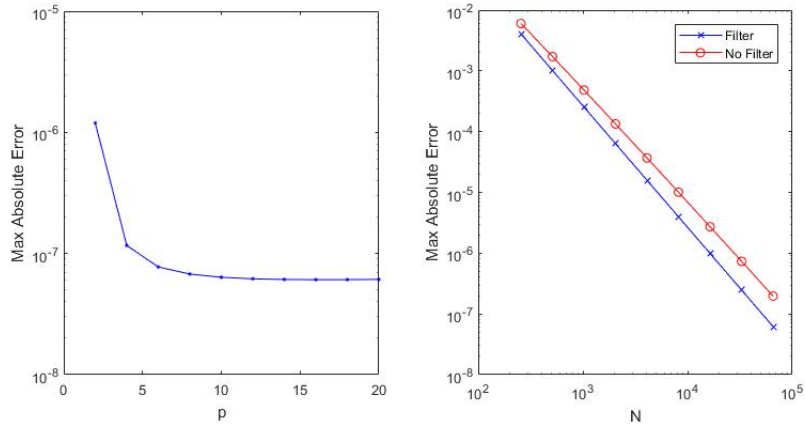


Figure 2.2: Effect of the filter on the Cauchy function. On the left, it is shown how the error decreases as  $p$  increases, for  $N = 2^{16}$ ; on the right, plot of the convergence of the error for  $N = 2^8, \dots, 2^{16}$  with  $p = 12$  and  $\Delta x = 2^{-3}$  with and without the filter application.

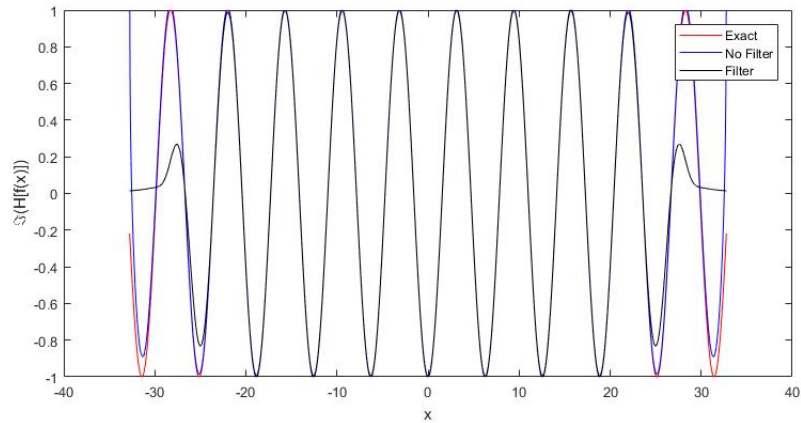


Figure 2.3: Plot of the imaginary part of the Hilbert Transform of  $f(x) = e^{ix}$ . With the filter the extrema are squeezed to 0, but it's possible to see that without the filter they are diverging.  $N = 2^{16}$ ,  $\Delta x = 2^{-10}$  and  $p = 30$  have been used.

the real and imaginary part of the function is improved by the application of the filter.

- c. In order to analyze the behaviour in case of discontinuities and asymptotic behaviours, we exploit the rectangular function with discontinuity near the extrema of our grid:

$$f(x) = \text{rect}(x) = \begin{cases} 0, & |x| \geq 40 \\ 1, & |x| < 40 \end{cases} \xrightarrow{\text{Hilbert}} \mathcal{H}[f(x)] = \frac{1}{\pi} \log \left| \frac{x+400}{x-400} \right|.$$

Indeed, choosing  $N = 2^{16}$  and  $\Delta x = 2^{-6}$ , the asymptotic behaviour at  $x = \pm 400$  will be at the extrema of our function. In this case, applying the

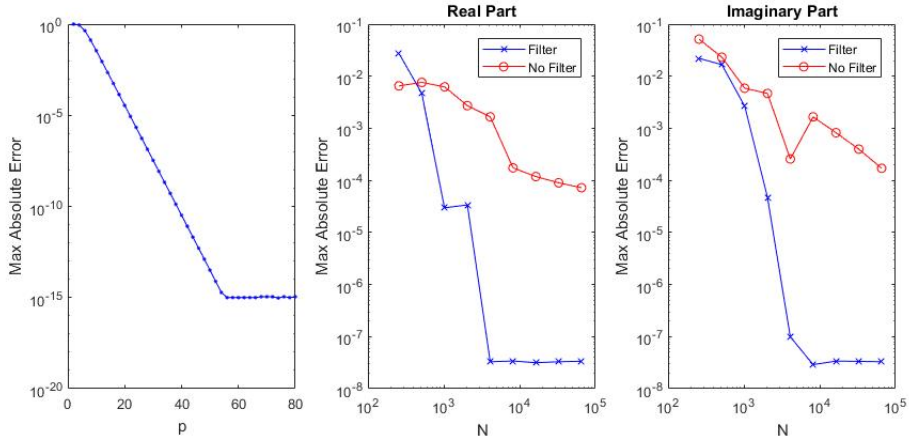


Figure 2.4: Effect of the filter on the Hilbert transform of  $f(x) = e^{ix}$ . On the left, it is shown how the error decreases as  $p$  increases, for  $N = 2^{16}$ ; in the other two plots, the convergence of the error for  $N = 2^8, \dots, 2^{16}$  with  $p = 30$  and  $\Delta x = 2^{-3}$  is shown for both the real and imaginary part of the Hilbert Transform.

filter has a double effect: near the discontinuity, it increase convergence, even if the error remains high; in the regular part of the function, the effect is the opposite. In this case, the suggestion is to erase the asymptotic behaviour, since its effect on the overall convergence of the method can be unpredictable, while the error in the regular part is anyway kept under control. We consider a value for  $p = 30$ , in order to minimize the error at the discontinuity.

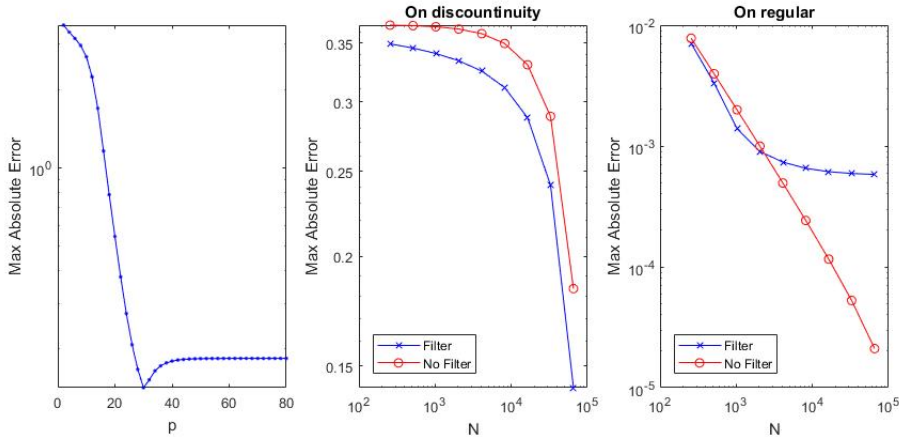


Figure 2.5: Effect of the filter on the Hilbert Transform of the rectangular function. On the left, it is shown how the error decreases as  $p$  increases, for  $N = 2^{16}$ ; in the other two plots, the convergence of the error for  $N = 2^8, \dots, 2^{16}$  with  $p = 30$  and  $\Delta x = 2^{-6}$  is shown for both the asymptotic and regular part of the Hilbert Transform.

We will analyze the error of this method for the computation of the Hilbert transform on the function  $h(z, s)$  in a similar way in section 3.3, but since



we don't have the exact solution to compare with, we will have to use some precautions.

## 2.3 Trapezoidal Rule for the Inverse Laplace

In this section, we expose the numerical method for the computation of the Inverse Laplace Transform, introduced by Abate and Whitt (1995).

**Proposition 2.2.** *Given a function  $\tilde{f}$  that doesn't contain singularities in the contour path defined by a real number  $a$ , the Inverse Laplace Transform  $f(t)$  of  $\tilde{f}$  can be approximated by the following expression:*

$$f(t) \approx \frac{e^{A/2}}{2t} \Re \tilde{f}(s_0) + \frac{e^{A/2}}{t} \sum_{k=1}^{\infty} (-1)^k \Re \tilde{f}(s_k),$$

where  $A = 2ta$  and  $s_k = \frac{A+2k\pi i}{2t}$ ,  $k \in \mathbb{N}$  (c.f. Eq. (5), Abate and Whitt (1995)).

*Proof.* (e.g. see Abate and Whitt (1995, p. 37)) First, let's start from definition 1.4 for a generic function  $f$ :

$$f(t) = \frac{1}{2\pi i} \int_{a-i\infty}^{a+i\infty} e^{st} \tilde{f}(s) ds.$$

Then, we move the integration on the real axis with a change of variables:

$$= \frac{1}{2\pi} \int_{-\infty}^{+\infty} e^{(a+iu)t} \tilde{f}(a+iu) du,$$

and rewriting the terms more explicitly, we get:

$$= \frac{e^{at}}{2\pi} \int_{-\infty}^{+\infty} (\cos(ut) + i \sin(ut)) (\Re[\tilde{f}(a+iu)] + i \Im[\tilde{f}(a+iu)]) du.$$

Exploiting some basic relations of complex calculus, such that  $\Re[f(a+ib)] = \Re[f(a-ib)]$  and  $\Im[f(a+ib)] = -\Im[f(a-ib)]$ , it's possible to derive the following expression:

$$= \frac{e^{at}}{\pi} \int_0^{\infty} (\cos(ut) \Re[\tilde{f}(a+iu)] - \sin(ut) \Im[\tilde{f}(a+iu)]) du,$$

and moreover, since in general  $\cos(x) \Re[f(x)] = -\sin(x) \Im[f(x)]$ :

$$= \frac{2e^{at}}{\pi} \int_0^{\infty} \cos(ut) \Re[\tilde{f}(a+iu)] du.$$

Finally, we use the trapezoidal rule to evaluate the integral, with step size  $h$ , getting:

$$f(t) \approx \frac{e^{at} h}{\pi} \Re[\tilde{f}(a)] + \frac{2e^{at} h}{\pi} \sum_{k=1}^{\infty} \cos(kht) \Re[\tilde{f}(a+ikh)].$$

Choosing  $h = \frac{\pi}{2t}$ , then  $\cos(kht) = (-1)^k$ ; therefore:

$$f(t) \approx \frac{e^{A/2}}{2t} \Re \tilde{f}(s_0) + \frac{e^{A/2}}{t} \sum_{k=1}^{\infty} (-1)^k \Re \tilde{f}(s_k).$$

■

The formula in proposition 2.2 is an approximation: the error implied in the discretization has been studied by Abate and Whitt (1995), resulting in the following bound that depends only on the chosen  $A$  if the function is continuous:

$$|\epsilon_d| \leq \frac{e^{-A}}{1 - e^{-A}}. \quad (2.5)$$

This result relies on the introduction of a periodic damped function  $g(t) = e^{-bt}f(t)$  with period  $T = 2\pi/h$  as the periodized version of  $f$  and its expansion in cosine Fourier series.

### 2.3.1 Euler Acceleration

According to proposition 2.2, the Inverse Laplace Transform should be computed truncating the series at a certain  $N$ . However, in order to improve the convergence of the alternating series, in Abate and Whitt (1995) the authors also apply the Euler Acceleration method, in addition to the trapezoidal rule. Following the notation in Phelan et al. (2018), define:

$$b_n = \frac{e^{A/2}}{2t} \Re \tilde{f}(s_0) + \frac{e^{A/2}}{t} \sum_{k=1}^n (-1)^k \Re \tilde{f}(s_k);$$

then the function  $f(t)$  can be approximated as:

$$f(t) \approx \frac{1}{2^{m_E}} \sum_{n=0}^{m_E} \binom{m_E}{n} b_{n_E+n},$$

i.e. taking the binomially weighted average of the terms  $b_n$  for  $n = n_E, \dots, n_E + m_E$ .

### 2.3.2 Numerical Tests

Since the payoff function we are going to price can go to 0 rapidly at expiry, we should consider the effect of this method for the inverse Laplace Transform on a discontinuous function, because the bound (2.5) is no more valid in presence of discontinuities (see Abate and Whitt (1992)).

For that reason, following the approach of Phelan et al. (2018), we are going to study the effect of the trapezoidal rule with Euler acceleration on the step function with delay, for example considering the function  $\tilde{f}(s) = \frac{e^{-10s}}{s}$ . In the figures 2.6, 2.7 and 2.8, we analyze the output of the algorithm for different values of  $A = 18.4, 23, 27$ , the trapezoidal rule parameter, and also of  $m_E$  and  $n_E$ , the Euler parameters (c.f. Fig. 2, 3, 4, Phelan et al. (2018, p. 215)). Indeed, we will have to choose appropriate values for  $m_E$  and  $n_E$ , balancing the error size with the time (and memory) required for the numerical computation of the binomial coefficients in the Euler acceleration formula.

In our applications, we will choose  $A = 23$ , in order to get an error floor of  $10^{-10}$  but not too much oscillation, and  $m_E = 61$ ,  $n_E = 100$  in order to reduce the size of the oscillations with a reasonable computation time for the binomial coefficient.

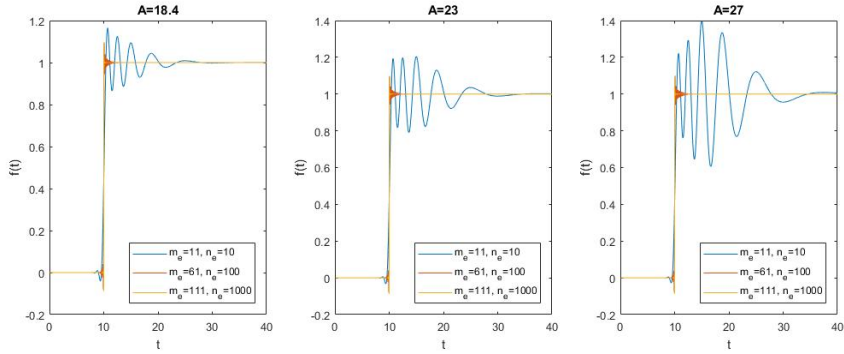


Figure 2.6: Inverse Laplace Transform of  $\tilde{f}(s) = \frac{e^{-10s}}{s}$  obtained with the method described. Increasing the Euler parameters reduces the size of oscillations, but  $A$  has the opposite effect.

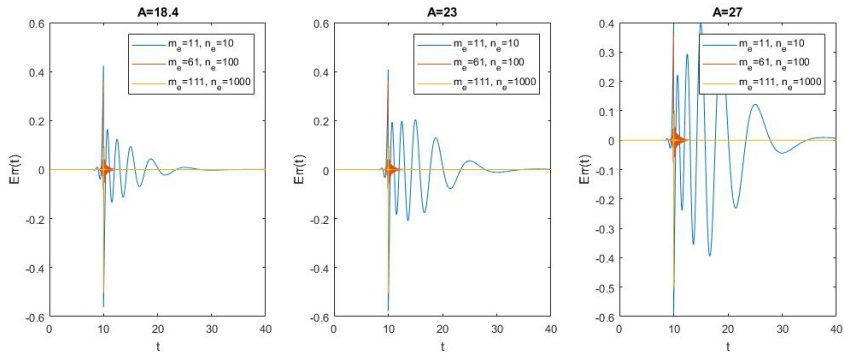


Figure 2.7: Error of the Inverse Laplace Transform of  $\tilde{f}(s) = \frac{e^{-10s}}{s}$  obtained with the method described. We can see the same behaviour as above.

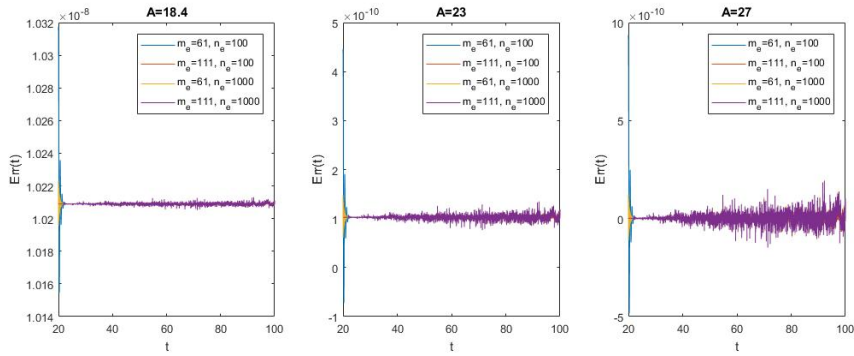


Figure 2.8: Noise in the tail of the error of the Inverse Laplace Transform of  $\tilde{f}(s) = \frac{e^{-10s}}{s}$  obtained with the method described. Increasing  $A$ , we reduce the size of the noise.

## Chapter 3

# Results of the Wiener-Hopf method

In this chapter we are going to present the results obtained with the Wiener-Hopf method for the pricing of exotic options introduced in this work. First, we briefly summarize the steps needed to obtain the results. Then, we study the effectiveness of the method comparing the price curve for different initial spots with the one obtained via closed formula in case of Brownian Motion. For the NIG model, we plot the results and compute the error with respect to the most precise result that can be obtained with the method. We apply the procedure both to the Fixed Strike Lookback Call Option and the Single Barrier Down & Out Call Option. In addition, we apply the method also to their digital versions. Moreover, we study the error convergence, with particular attention to the error induced by the Sinc Expansion method. Finally, we analyze the effect of the damping parameter, confirming the existence of an analyticity strip.

### 3.1 Pricing Procedure

Following the approach of Phelan et al. (2018), we sum up the steps to be followed for the numerical computation of the options' prices.

1. Set up the three different grids for each transform domain: the grid of  $\{x_l\}$  for the real domain, the grid of  $\{z_j\}$  for the Fourier (and Hilbert) Transform and the grid of  $\{s_k\}$  for the Laplace Transform. According to sections 2.1 and 2.3:

$$\begin{cases} \{x_l\} = -\frac{N-1}{2}\Delta x, \dots, \frac{N-1}{2}\Delta x, \\ \{z_j\} = -\frac{N-1}{2}\Delta z, \dots, \frac{N-1}{2}\Delta z \end{cases}, \quad \{s_k\} = \frac{A + 2\pi k i}{2T},$$

with  $\Delta x \Delta z = \frac{2\pi}{N}$ ,  $N$  is a power of 2 and  $i$  is the imaginary unit.

2. Compute the values of the characteristic exponent for each  $z_j$  as  $\psi(z_j + i\gamma)$ , where  $\gamma$  is the damping parameter. Then, set the function to be decomposed:  $h(z_j + i\gamma, s_k) = \log(s_k - \psi(z_j + i\gamma))$ .
3. Apply the Sinc Expansion method in order to compute the Hilbert Transform needed in the decomposition:

- In case of Lookback, find the Wiener-Hopf factors  $h(z_j + i\gamma, s_k) = h_+(z_j + i\gamma, s_k) + h_-(z_j + i\gamma, s_k)$  and get the Laplace Transform of the characteristic function for the maximum as:

$$\widetilde{p}^M(z_j + i\gamma, s_k) = \frac{1}{e^{h_+(z_j + i\gamma, s_k) + h_-(0, s_k)}}.$$

- In case of Single Lower Barrier B, first find the Wiener-Hopf factors  $h(z_j + i\gamma, s_k) = h_+(z_j + i\gamma, s_k) + h_-(z_j + i\gamma, s_k)$ ; then, decompose at the lower log-barrier  $b = \log(B/S_0)$  the function  $j(z_j + i\gamma, s_k) = 1/\exp(h_-(z_j + i\gamma, s_k)) = j_{b+}(z_j + i\gamma, s_k) + j_{b-}(z_j + i\gamma, s_k)$  using the Plemelj-Sokhotsky relations and get the Laplace Transform of the characteristic function for the process with lower barrier as:

$$\widetilde{p}^{(b)}(z_j + i\gamma, s_k) = \frac{j_{b+}(z_j + i\gamma, s_k)}{e^{h_+(z_j + i\gamma, s_k)}}.$$

4. Multiply the result by complex conjugate of the damped payoff function  $\phi_\gamma^*(z_j)$  and apply the FFT procedure of section 2.1, getting as output a function  $\tilde{f}(x_l, s_k)$ .
5. Apply the trapezoidal rule with Euler acceleration to the output, as in section 2.3, in order to get a function  $f(x_l, T)$ .
6. Finally, the option price is equal to the function  $f$  evaluated at  $x = 0$ .

As in Phelan et al. (2018), the parameters for the options are strike price  $K = 1.1$  and, in the case of barrier option, lower barrier  $B = 0.8$ . The maturity of the options is  $T = 1$ ; a risk-free rate of  $r = 0.05$  and a dividend yield of  $q = 0.02$  are assumed. In the following sections, we will price the option for different possible values of the initial spot price of the asset  $S_0$ . Notice that the first part of the algorithm, involving the factorization of  $h$ , is the same for each spot; then, it changes for each initial spot in the factorization of  $j$  and in the multiplication by the payoff function. We divide the analysis on the basis of the underlying Lévy process assumed.

### 3.1.1 Brownian Motion model

If the process of log-returns is modelled with a Brownian Motion with drift, we apply the algorithm proposed above to the characteristic exponent:

$$\psi_{BM}(z) = i\mu z - \frac{1}{2}\sigma^2 z^2.$$

Choosing  $\mu = r - q - \sigma^2/2$ , we are considering the risk-neutral measure of the Black & Scholes model in presence of dividend yield, therefore one can apply the analytical formulas of section 1.5 in order to find the options' prices. We use the closed formulas' results as reference values, selecting  $\sigma = 0.2$ .

The idea is to compute the curve of prices with different initial spots and compare the prices obtained with the Wiener-Hopf method with the ones got via closed formula. In figure 3.1 it is shown that the method actually converges to the right result, while in figure 3.2 we study the absolute error made across

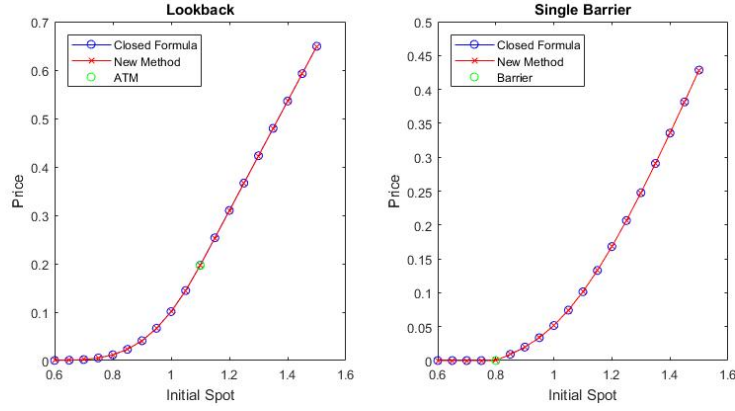


Figure 3.1: Prices for Lookback (left) and Single Barrier Option (right) with different initial spot under the BM Model. We consider initial spot prices  $S_0 = 0.6, \dots, 1.5$ , grid size  $N = 2^{16}$  and  $\Delta z = 2^{-2}$ . Damping parameter  $\gamma = -3$ .

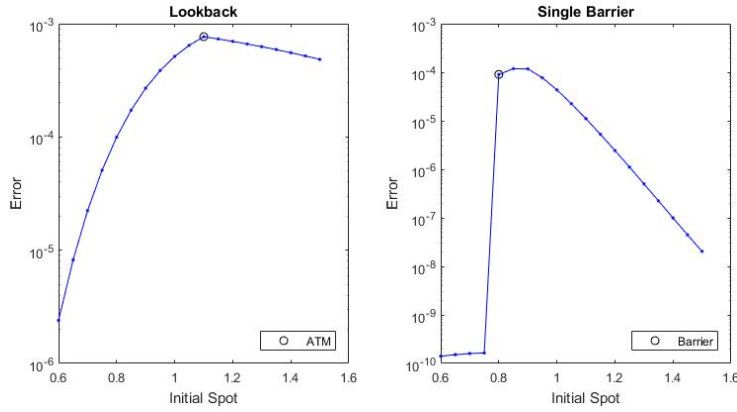


Figure 3.2: Absolute Error for Lookback (left) and Single Barrier Option (right) with different initial spot under the BM Model. We consider initial spot prices  $S_0 = 0.6, \dots, 1.5$ , grid size  $N = 2^{16}$  and  $\Delta z = 2^{-2}$ . Damping parameter  $\gamma = -3$ .

the curve.

For the lookback, the error is maximum for the At-the-money option, where the strike price falls exactly at the decomposition point for  $h(z, s)$ . In this case, the maximum error is lower than  $10^{-3}$ . For the barrier option, the maximum error is reached around the barrier, since this is the problematic point with discontinuity in the payoff. The maximum error has the order of magnitude of  $10^{-4}$ , but the error almost vanishes below the barrier level. A more detailed analysis about the error and its convergence is considered in section 3.2.

### Digital Options

We saw in section 1.4 that the method can be applied also to the digital version of the options. In figures 3.3 and 3.4, we show the results on the Digital

with lower barrier and the American Digital option for the Brownian Motion model for log-returns, that have been introduced with their closed formulas in section 1.5. The behaviour of the error is similar in the barrier option case, while the structure is different in the American Digital, since the price of the digital option is constant for  $S_0 \geq K$ , as the option will pay 1 for sure. Moreover, the magnitude of the maximum error is a bit higher, being in both cases around  $10^{-3}$ .

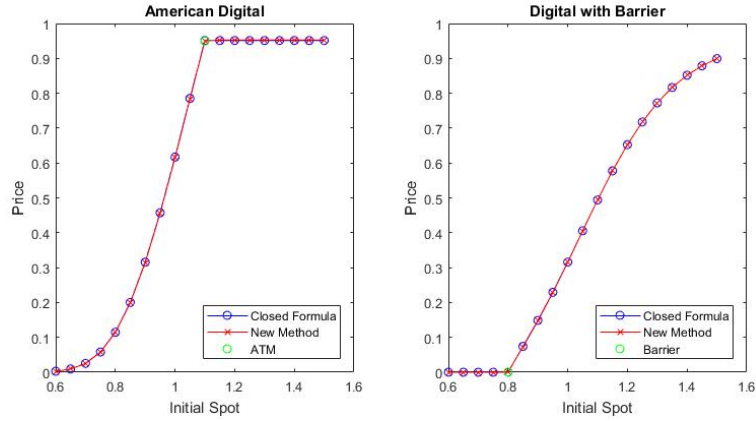


Figure 3.3: Prices for American Digital (left) and Digital with Barrier (right) with different initial spot under the BM Model. We consider initial spot prices  $S_0 = 0.6, \dots, 1.5$ , grid size  $N = 2^{16}$  and  $\Delta z = 2^{-2}$ . Damping parameter  $\gamma = -3$ .

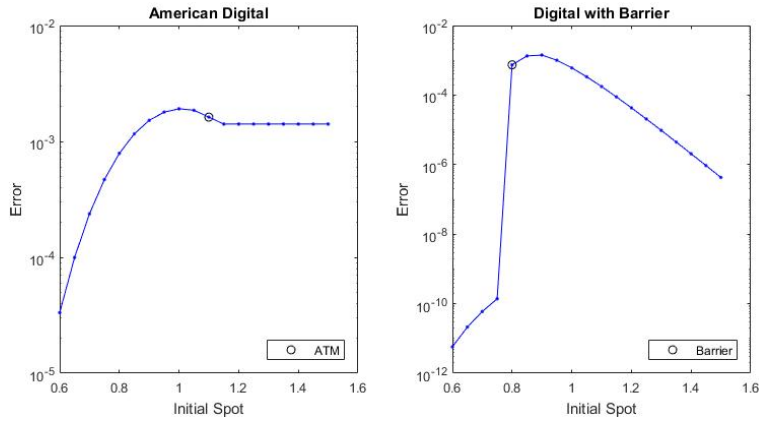


Figure 3.4: Absolute Error for American Digital (left) and Digital with Barrier (right) with different initial spot under the BM Model. We consider initial spot prices  $S_0 = 0.6, \dots, 1.5$ , grid size  $N = 2^{16}$  and  $\Delta z = 2^{-2}$ . Damping parameter  $\gamma = -3$ .

### 3.1.2 NIG Model

The second kind of Lévy Process considered in this work is the Normal Inverse Gaussian process, which is characterized by characteristic exponent:

$$\psi_{NIG}(z) = i\mu z + \delta(\gamma - \sqrt{\alpha^2 - (\beta + iz)^2}),$$

where  $\gamma = \sqrt{\alpha^2 - \beta^2}$ , with  $\delta > 0$  and  $0 \leq |\beta| \leq \alpha$ , where the risk-neutral measure is recovered choosing:

$$\mu = r - q - \delta(\gamma - \sqrt{\alpha^2 - (\beta + 1)^2}).$$

Differently from before, we don't have a closed formula to compare the results with: in order to have a figure of the magnitude of the error implied in the method, we compare the results obtained with a grid of  $N = 2^{15}$  points with the the ones obtained with  $N_{\max} = 2^{16}$ , which is our grid limit. The choice of the parameters for the NIG distribution is made according to Phelan et al. (2018), with  $\alpha = 15$ ,  $\beta = -5$  and  $\delta = 0.5$ . As in the Brownian Motion case, we study the behaviour of the method for different initial spots.

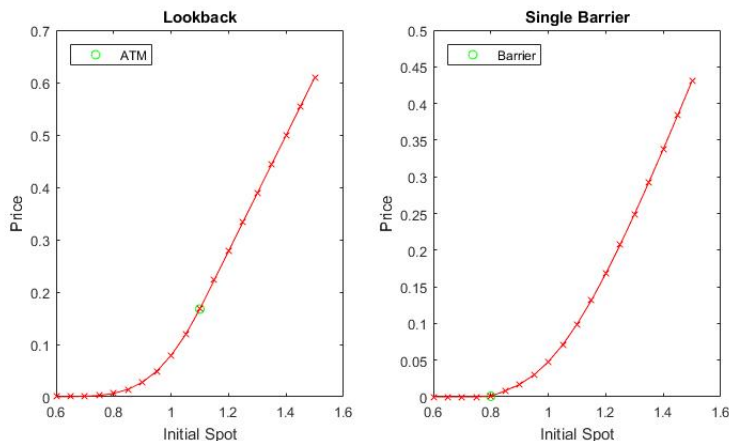


Figure 3.5: Prices for Lookback (left) and Single Barrier Option (right) with different initial spot under NIG model. We consider initial spot prices  $S_0 = 0.6, \dots, 1.5$ , grid size  $N = 2^{15}$  and  $\Delta z = 2^{-2}$ . Damping parameter  $\gamma = -3$ .

In figure 3.5, we can see that the prices varying  $S_0$  have the same behaviour as in the Brownian Motion case. Moreover, the error between the two approximations is very similar to the previous case both for shape and order of magnitude: in figure 3.6 we see a maximum error at the ATM option smaller than  $10^{-3}$  for the lookback and a maximum error at the barrier level around  $10^{-4}$  for the single barrier option.



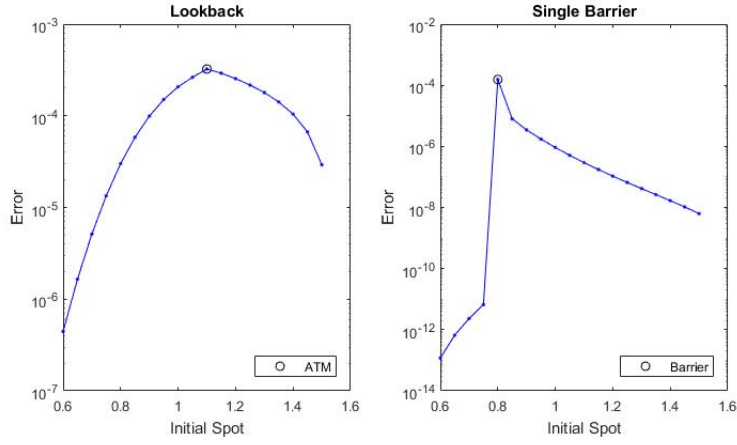


Figure 3.6: Absolute Error for Lookback (left) and Single Barrier Option (right) with different initial spot under NIG model between grid size  $N = 2^{15}$  and maximum grid size  $N_{\max} = 2^{16}$ . We consider initial spot prices  $S_0 = 0.6, \dots, 1.5$ ,  $\Delta z = 2^{-2}$  and damping parameter  $\gamma = -3$ .

### Digital Options

As for the study on the Brownian Motion model, we propose the results for the digital versions of the lookback and barrier options. Also in this case, the error is computed comparing the values obtained with  $N = 2^{15}$  with the ones got with  $N_{\max} = 2^{16}$ . For both the digital options, the magnitude of the error is the same as under the Brownian Motion model.

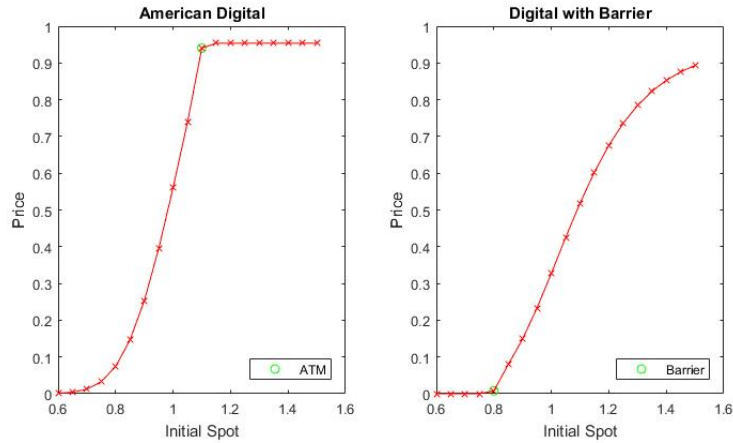


Figure 3.7: Prices for American Digital (left) and Digital with Barrier (right) with different initial spot under NIG model. We consider initial spot prices  $S_0 = 0.6, \dots, 1.5$ , grid size  $N = 2^{15}$  and  $\Delta z = 2^{-2}$ . Damping parameter  $\gamma = -3$ .

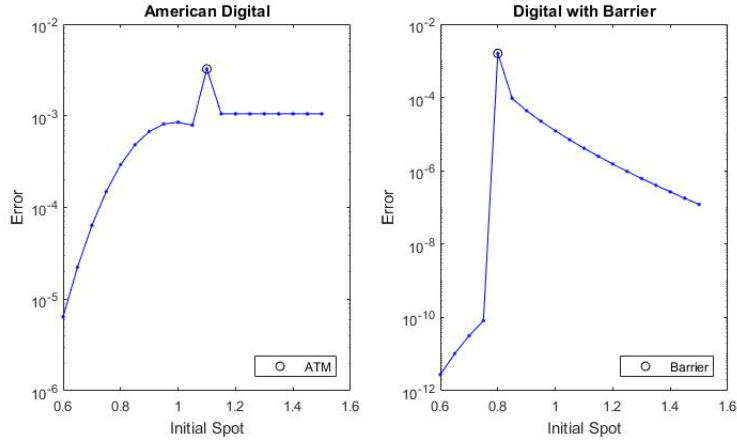


Figure 3.8: Absolute Error for American Digital (left) and Digital with Barrier (right) with different initial spot under NIG model between grid size  $N = 2^{15}$  and maximum grid size  $N_{\max} = 2^{16}$ . We consider initial spot prices  $S_0 = 0.6, \dots, 1.5$ ,  $\Delta z = 2^{-2}$  and damping parameter  $\gamma = -3$ .

### 3.2 Error Convergence

Up to now, we have studied the error on the complete curve of prices, but with a certain fix grid size: for the Brownian Motion,  $N = 2^{16}$ , since we have a closed formula as reference value, while for the NIG model we used  $N = 2^{15}$  in order to use the thicker grid as reference. However, it is also important to understand the rate of convergence of the method with  $N$ , i.e. how the error decays by increasing the number of points in the grid. In order to study this behaviour, we can compare the price of the option computed with different values of  $N$  to the reference value.

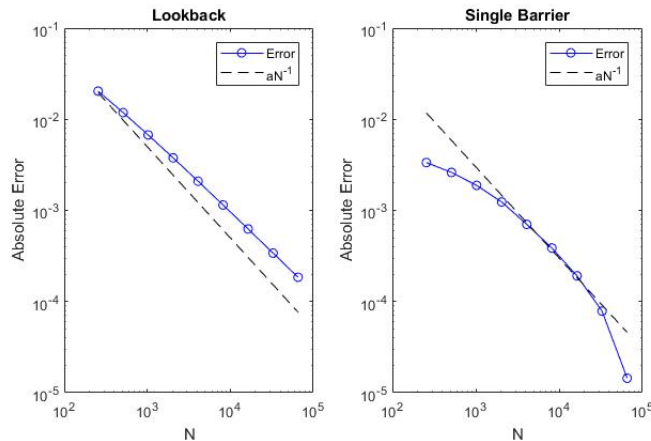


Figure 3.9: Plot in log-log scale of the Absolute Error of the method with the Brownian Motion model for different  $N = 2^8, \dots, 2^{16}$  for the lookback (left) and the single barrier option (right).  $\Delta z = 2^{-2}$  and damping parameter  $\gamma = -3$ . The reference values are computed via closed formulas.

In particular, we choose as initial spot  $S_0 = 0.81$ , since the most discontinuous movement of the error is at the barrier level for the barrier option, while for the lookback the curve of errors doesn't present jumps. Moreover, in this way we are looking at errors with the same order of magnitude, which is in both cases a bit smaller than  $10^{-4}$ .

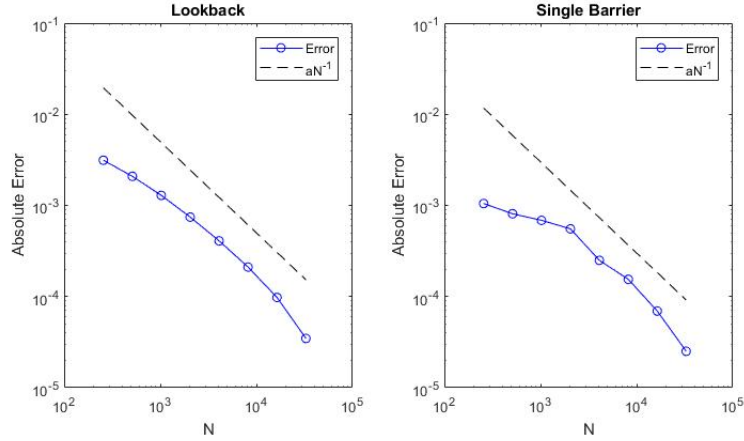


Figure 3.10: Plot in log-log scale of the Absolute Error of the method with the NIG model for  $S_0 = 0.81$  for different  $N = 2^8, \dots, 2^{15}$  for the lookback (left) and the single barrier option (right).  $\Delta z = 2^{-2}$  and damping parameter  $\gamma = -3$ . The reference values are computed via Wiener-Hopf method with  $N_{\max} = 2^{16}$ .

In figures 3.9 and 3.10, the convergence results with respect to the number of grid points are shown. For the BM model, the method has been applied with  $\Delta z = 2^{-2}$ , for numbers of grid points  $N = 2^8, \dots, 2^{16}$ ; for the NIG model, we use  $N = 2^8, \dots, 2^{15}$  and the same  $\Delta z$ . Notice that the error has a decay rate which is slightly slower than  $N^{-1}$ .

In addition to the analysis done for the convergence with the number of points  $N$ , we also have to consider the other parameter of the FFT, i.e. the grid step size, that we have chosen as  $\Delta z = 2^{-2}$ . This choice is not arbitrary: let's analyze the behaviour of the absolute error for the different options as  $\Delta z$  changes, considering  $N = 2^{16}$ . As in the previous case, we consider only the lookback and single barrier options with initial spot  $S_0 = 0.81$ , since the analysis is similar in the digital cases.

Due to the structure of the FFT algorithm and the connection of the two grids  $\{x_l\}$  and  $\{z_k\}$ , the behaviour of the error must be handled carefully. Indeed, if we consider a small  $\Delta z$  we are taking a small interval in the transformed space, while if we take  $\Delta z$  too high the problem is moved on the real space: in both cases, we are making a bad approximation of the integral. Moreover, we also have to consider the error that can be made in the computation of the Hilbert Transform with the Sinc Expansion due to the choice of  $\Delta z$  and the use of the filter introduced in section 2.2.2, which is analyzed separately in section 3.3. We analyze only the Brownian Motion case, since the behaviour of the error is not convergent in this case and therefore we can't use as reference a value computed

with the method itself for the NIG model.

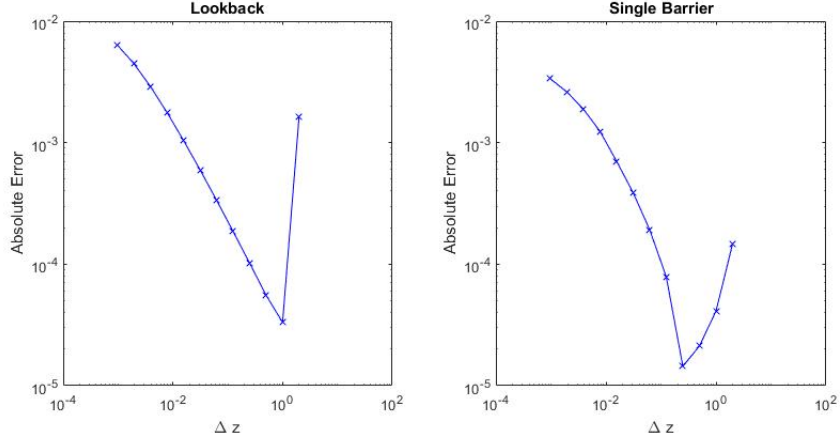


Figure 3.11: Plot in log-log scale of the Absolute Error of the method with the Brownian Motion model for  $S_0 = 0.81$  for different  $\Delta z = 2^{-10}, \dots, 2^1$  for the lookback (left) and the single barrier option (right).  $N = 2^{16}$  and damping parameter  $\gamma = -3$ . The reference values are computed via closed formulas.

In figure 3.11 for the BM model, it is possible to see how the error decreases as  $\Delta z$  increases up to a certain point, after which the error increases again and with a higher speed, showing a certain instability. Looking at the two options separately, we have as limit case  $\Delta z = 2^0$  for the lookback option and  $\Delta z = 2^{-2}$  for the single barrier option, at which the error is minimized. In both cases, choosing  $\Delta z$  in the interval  $[0.25, 1]$  assures an error smaller than  $10^{-4}$ . We decided to take  $\Delta z = 2^{-2}$  in order to be in the safe and not unstable part of the error for the single barrier option.

### 3.3 Analysis of the Sinc Expansion

In section 2.2, some numerical tests were performed on test functions in order to check the behaviour of the approximation of the Hilbert Transform through the Sinc Expansion. In those cases, the analytic form of the Hilbert Transform was known, therefore it was possible to compute a reference value and to check the convergence of the absolute error implied in the expansion. We would like to proceed in a similar way for the function that we have to decompose, i.e.  $h(z, s)$ . First, we study the properties of this function, checking graphically the existence of an analyticity strip in which we can apply proposition 2.1, and then we look at the error obtained when we apply the Sinc expansion formula.

Consider:

$$h(z, s) = \log(l(z, s)) = \log(s - \psi(z)), \quad s, z \in \mathbb{C}.$$

The analyticity strip of the function can be studied considering that the logarithm is an analytic function on  $\mathbb{C} - \mathbb{R}_{\leq 0}$ , i.e. on the whole complex plane

cutting the negative part of the real axis. Therefore, we have to focus on the argument of the logarithm  $l(z, s)$  and understand for which values of  $s$  and  $z$  this function has values on the complex plane without touching the line  $\mathbb{R}_{\leq 0}$ . In particular, we would like to find a strip of complex  $z$  for which the condition above is satisfied, in order to apply proposition 2.1.

First, let's consider the variable  $s$ : the choice for the grid  $\{s_k\}$  takes points all with the same real part, equal to  $\Re(s_k) = \frac{A}{2T}$ , and an imaginary part  $\Im(s_k) = \frac{2k\pi}{2T}$  that has the only effect of shifting up  $\Im(l(z, s))$  as  $k$  increases. In figure 3.12, we plot the values on the complex plane that can be obtained for  $l(z, \frac{A}{2T}) = \frac{A}{2T} - \psi(z)$  considering  $z$  taking values on the real axis as in the grid  $\{z_j\}$ .

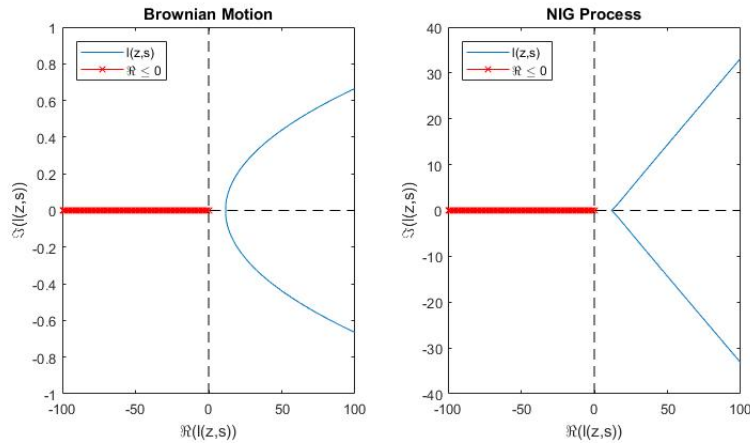


Figure 3.12: Plot of  $l(z_k, A/2T)$  on the complex plane for  $A = 23$ ,  $T = 1$  under Brownian Motion model (left) and NIG model (right). Grid size  $N = 2^{16}$ ,  $\Delta z = 2^{-2}$ .

It is possible to see that the effect of the imaginary part of  $s$  doesn't affect the condition of touching the negative part of the real line, since, as said, it only shifts up the curve in the plane. For that reason, in the following analysis we take  $s = \frac{A}{2T}$  as a parameter and focus on  $z$ .

Since we want to find a strip of  $z$  such that  $\{z \in \mathbb{C} : |\Im(z)| < d\}$ , we consider of shifting our real grid of  $\{z_j\}$  of an arbitrary imaginary part  $c$  for different values of  $c \in \mathbb{R}$ . Thus, we consider the function  $l(z_j + ic, A/2T)$  and look for the satisfaction of the condition for  $c$  in a range  $[-d, d]$ . From figure 3.13, in the Brownian Motion case it is easy to see that a strip actually exists, since in the case presented we are not touching  $\mathbb{R}_{\leq 0}$  up to  $c = \pm 23$ . Also in the NIG case a similar range can be found, even if the shape of the function is less regular. Of course, the exact values of these ranges depend on the parameters used for the two characteristic exponents and on the Laplace parameters, which we are considering as in the previous sections 3.1 and 3.2.

This graphical analysis assures that the function  $h(z, s)$  is analytic at least in a strip of the complex plane  $[-d, d]$ , with  $d$  depending on the parameters chosen; therefore it satisfies the hypothesis of proposition 2.1, assuring an exponential

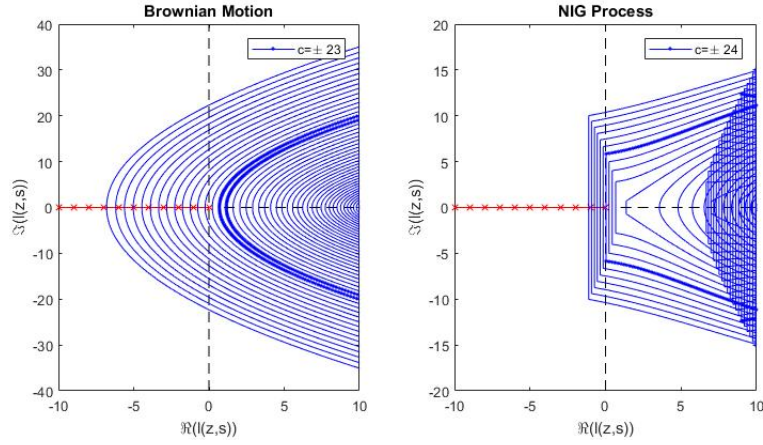


Figure 3.13: Plot of  $l(z_k + ic, A/2T)$  on the complex plane for  $A = 23$ ,  $T = 1$  under Brownian Motion model (left) and NIG model (right) for  $c \in [-30, 30]$ . Grid size  $N = 2^{16}$ ,  $\Delta z = 2^{-2}$ .

decay of the error of the approximation. Let's recall that we are interested in the computation of the function  $h(z, s)$  for  $z = z_j + i\gamma$ ,  $\gamma < -1$ : thus, as we will numerically confirm in section 3.4, one can choose  $\gamma \in [-d, -1)$  without affecting the speed of convergence.

As said, we want to study the convergence of the results of the Sinc Expansion method. We will perform our analysis only on the Brownian Motion case, as the NIG process case will lead to similar results. Since we don't have an analytic result for the transformed function, we can only study the convergence of the method using as reference value the one obtained with the thickest grid ( $N = 2^{16}$  in our applications).

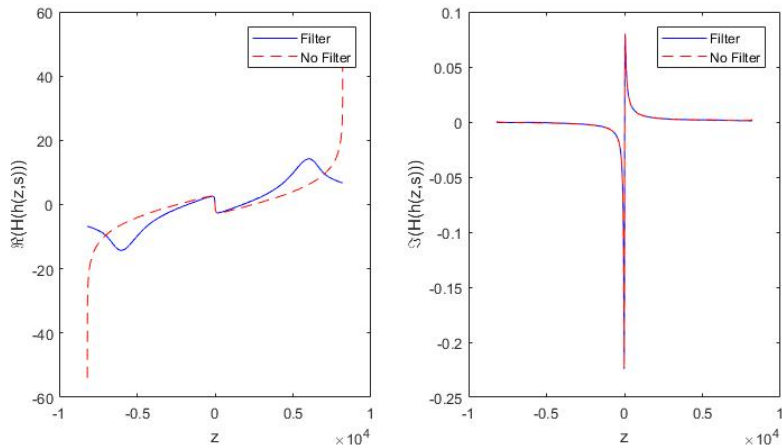


Figure 3.14: Plot of the real (left) and imaginary (right) parts of the Hilbert Transform of  $h(z, s)$  in the Brownian Motion case computed with  $N = 2^{16}$ ,  $\Delta z = 2^{-2}$ .

Moreover, plotting the real and imaginary part of the transformed function as in figure 3.14, we notice that the real part has diverging tails: for that reason, the application of the exponential filter is needed to recover the correct convergence. Since we have this diverging behaviour at the tails, we should handle the comparison between different grids very carefully: when comparing the results coming from grids with different number of points or step size, the total interval covered by each grid must be the same. We will focus on two different kind of convergence. First, we analyze the convergence of the method keeping the same interval covered (i.e.  $z_{\min} = -z_{\max}$  are kept constant) but increasing the number of points in the grid. Our reference value will be computed with  $N_{\max} = 2^{16}$  and  $\Delta z_{\min} = 2^{-2}$ . Then, the convergence is studied for  $N_k = 2^8, \dots, 2^{15}$ : in order to keep the same interval, one should choose accordingly:

$$\Delta z_k = \frac{N_{\max} - 1}{N_k - 1} \Delta z_{\min}. \quad (3.1)$$

In figure 3.15 the convergence of the absolute error with or without the filter is compared for both the real and imaginary part. Clearly, we see that in particular on the real part the filter has a great effect on the maximum absolute error, since the diverging tail part is canceled. On the other hand, we see how the method is highly convergent thanks to the application of the filter as the number of points in the grid is increased.

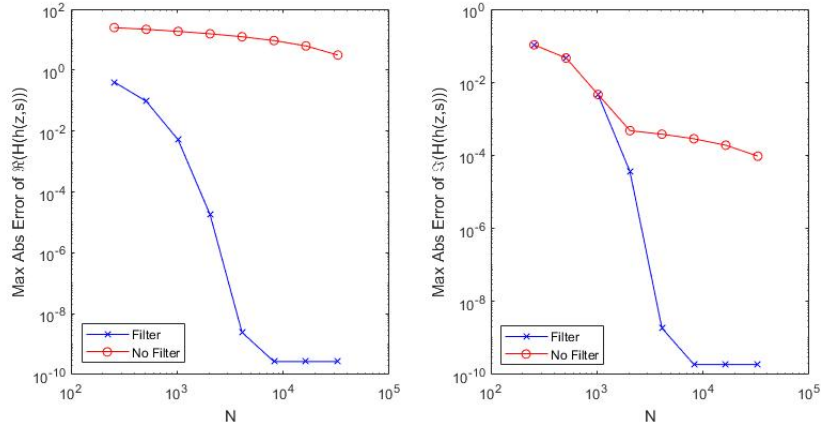


Figure 3.15: Plot of Max Absolute Error for the real (left) and imaginary (right) parts of the Hilbert Transform of  $h(z, s)$  in the Brownian Motion case for different values of  $N$ .

We also want to study the convergence of the method using the same number of points, but considering different total intervals covered, i.e. different step sizes between the points. We expect the error to converge as  $\Delta z$  decreases. For each  $\Delta z$ , we compare the result obtained with  $N = 2^{15}$  with the one obtained with  $N = 2^{16}$  on the same interval, i.e. we choose for each  $\Delta z_{16}$  used for the reference value a  $\Delta z_{15}$  selected according to formula (3.1). In figure 3.16, we used  $\Delta z_{16} = 2^{-12}, \dots, 2^0$ . The filter has a huge effect this time, in particular on the imaginary part that has an asymptotic behaviour near  $z = 0$ . Without the filter, the error is not convergent with  $\Delta z$ . Therefore, in our application we will

use the exponential filter, so that the error induced by the Hilbert Transform computation won't affect the overall behaviour of the complete method.

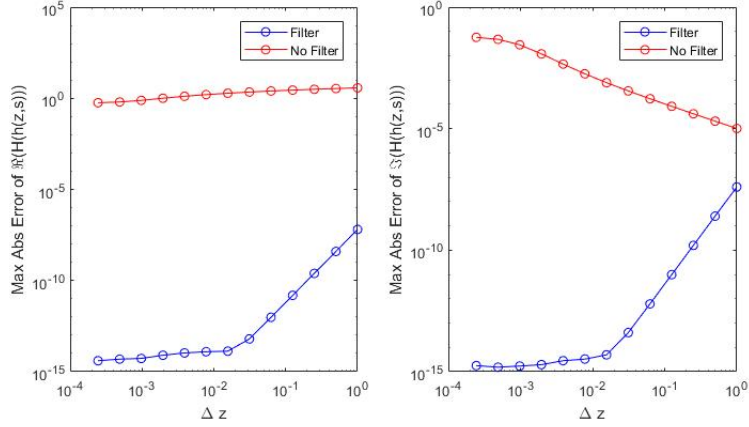


Figure 3.16: Plot of Max Absolute Error for the real (left) and imaginary (right) parts of the Hilbert Transform of  $h(z, s)$  in the Brownian Motion case for different values of  $\Delta z$ .

### 3.4 Analysis of the damping parameter

As we saw in the previous section, the analyticity strip of the function to which we apply the Sinc Expansion for the Hilbert Transform depends on the parameters of the model chosen and on the value of the real part of the grid for the Inverse Laplace Transform. Moreover, when we introduce the damping parameter, we are actually shifting the axis of integration (i.e. the real axis) up or down on the complex plane of  $\gamma$  imaginary units: we should check that we are always moving the axis inside the analyticity strip of the decomposed function  $h(z, s)$ , otherwise the results do not converge. Therefore, we can only choose  $\gamma \in [-d, -1)$ , where  $d$  is the maximum radius of the complex part of the analyticity strip.

In order to verify the existence and the interval of analyticity, we can compute the option price with initial spot  $S_0 = 0.81$  for different values of  $\gamma$  and observe if we notice a stability region. Notice that since the stability region is not affected by the number of points in the grid  $N$ , we choose  $N = 2^{14}$  in order to speed up the computation.

In figure 3.17 it's clear that the analysis we did on the function is correct: the result is stable for  $\gamma \in [-23, -1)$ . Out of this interval, the price has a sudden jump. In figure 3.18, the analyticity region for the NIG model is analyzed. The parameters for the characteristic exponent are chosen as in the previous sections. One can notice that the strip is smaller, since we can choose only up to  $\gamma = -19$  to be in the stability region, since we are using  $\alpha = 15$ ,  $\beta = -5$  and according to the study of Feng and Linetsky (2008) the damping parameter should be chosen in the interval  $\gamma \in [\beta - \alpha, \beta + \alpha]$  for the analyticity of the



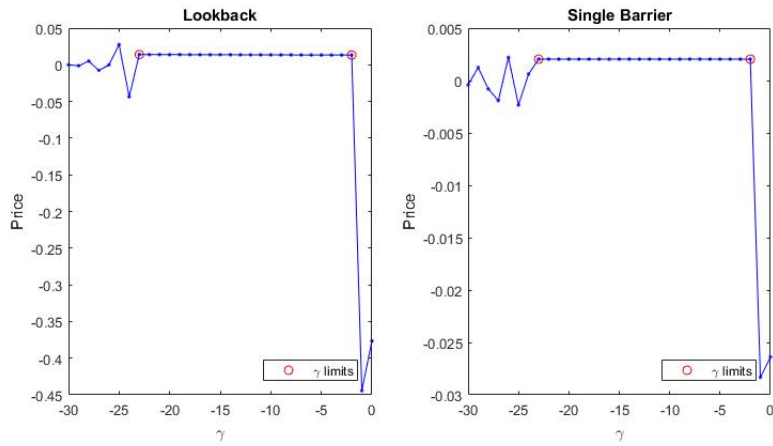


Figure 3.17: Option Prices for Lookback (left) and Single Barrier Option (right) for different values of  $\gamma = -30, \dots, 0$  for the Brownian Motion Model. The Wiener-Hopf method has been applied with  $N = 2^{14}$  and  $\Delta z = 2^{-2}$ .

Characteristic Exponent.

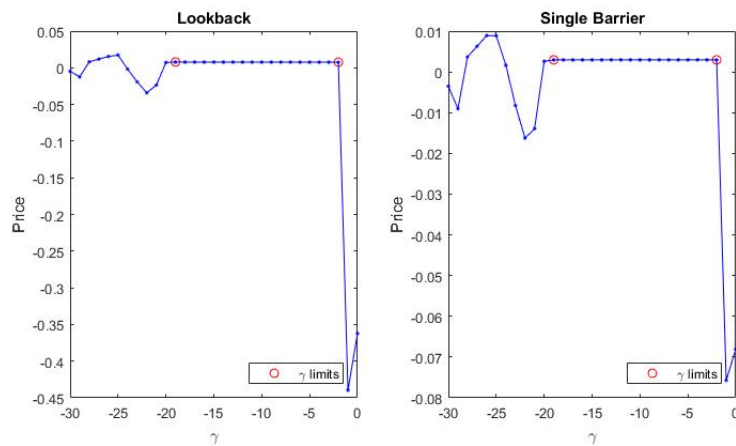


Figure 3.18: Option prices for Lookback (left) and Single Barrier Option (right) for different values of  $\gamma = -30, \dots, 0$  for the NIG Model. The Wiener-Hopf method has been applied with  $N = 2^{14}$  and  $\Delta z = 2^{-2}$ .

### Digital Options

The same analysis can be done for the digital versions of the options. In particular, as we saw in section 1.4, the damping parameter for the payoff must be  $\gamma < 0$ , therefore values of the damping parameters can be chosen for  $\gamma \in [-d, 0)$ . In figures 3.19 and 3.20, it is possible to verify the stability region for

the price as mathematically derived, since also the value  $\gamma = -1$  is stable. The value of  $d$  is exactly the same as in the previous cases, since the digital feature impacts only on the payoff function.

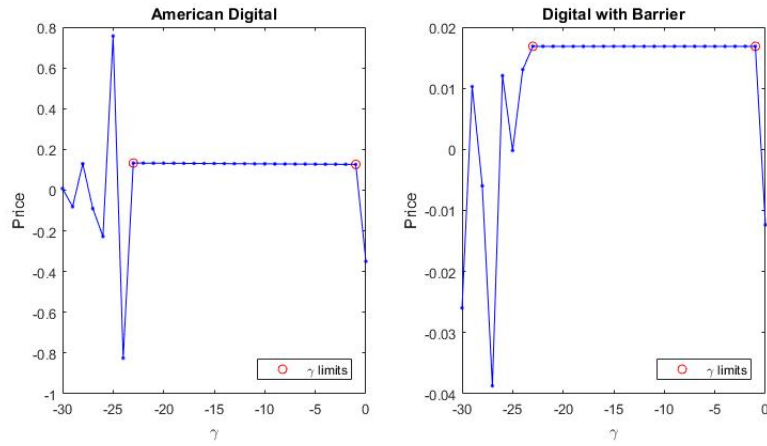


Figure 3.19: Option Prices for American Digital (left) and Digital with Barrier (right) for different values of  $\gamma = -30, \dots, 0$  for the Brownian Motion Model. The Wiener-Hopf method has been applied with  $N = 2^{14}$  and  $\Delta z = 2^{-2}$ .

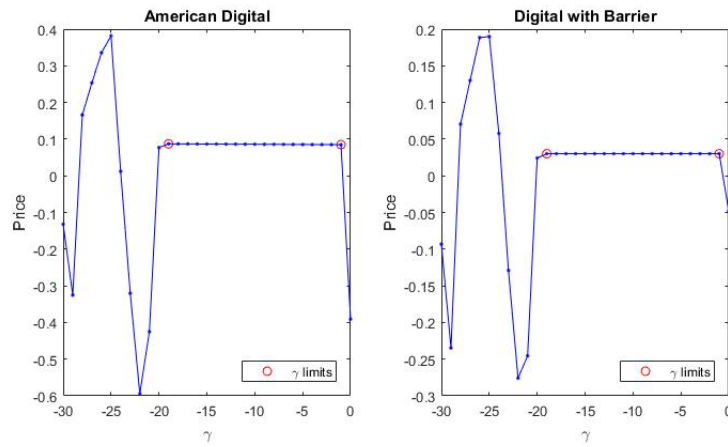


Figure 3.20: Option Prices for American Digital (left) and Digital with Barrier (right) for different values of  $\gamma = -30, \dots, 0$  for the NIG Model. The Wiener-Hopf method has been applied with  $N = 2^{14}$  and  $\Delta z = 2^{-2}$ .

## Chapter 4

# A New Monte Carlo Method

The method introduced in the previous chapters can be applied to some of the most well-known Lévy processes, as performed in Phelan et al. (2018) on single and double barrier options. However, the presented method relies on complex mathematical procedures, such as the Wiener-Hopf decomposition or the inversion of some complex transforms. In general, the simplest way for pricing path-dependent options is to rely on Monte Carlo simulations. Even though it may be time-consuming, this approach is easy to implement, since it only requires the simulation of  $N$  underlying paths and then to take the mean of all possible outcomes.

In this chapter, following the approach of Alabert and Caballero (2018) and relying on the study of Becker (2010), we introduce a new method for the simulation of the maximum (or minimum) of a Brownian Motion, fixing the problems of convergence embedded in the traditional Monte Carlo simulation method. The new method can be applied both to lookback and single barrier options; moreover, it can be applied not only to the Brownian Motion model for log-returns, but also to the NIG model, as we will show.

### 4.1 Brownian Motion

In the case of Brownian Motion, the distribution of its extrema is well-known. Moreover, thanks to the fact that the joint distribution of the Brownian Motion and its maximum is known in analytical form, it's also possible to derive the distribution of the maximum (or the minimum) for a Brownian Bridge. First, let's introduce the mathematical framework for the Brownian Motion case.

**Definition 4.1** (Brownian Motion). *A standard Brownian Motion is a real-valued stochastic process  $\{W_t\}_{t \geq 0}$  such that:*

- $W_0 = 0$  a.s.;
- $W_t - W_s \sim W_{t-s} \sim \mathcal{N}(0, t - s)$ ,  $0 \leq s < t$ , i.e.  $W$  has stationary increments, normally distributed;
- Given  $0 \leq t_1 < \dots < t_n$ , then  $W_{t_1}, W_{t_2} - W_{t_1}, \dots, W_{t_n} - W_{t_{n-1}}$  are independent;

- $t \mapsto W_t$  is continuous a.s. on  $[0, \infty)$ .

Given this definition, we can introduce the more general case of the Brownian Motion with drift  $\mu$  and diffusion parameter  $\sigma$ :

$$X_t = \mu t + \sigma W_t.$$

It's easy to understand that  $X_t$  is normally distributed with mean  $\mu t$  and variance  $\sigma^2 t$ . For that reason, the probability density function of the stochastic process  $X_t$  is given by:

$$f_{X_t}(x) = \frac{1}{\sqrt{2\pi\sigma^2 t}} e^{-\frac{(x-\mu t)^2}{2\sigma^2 t}}.$$

## 4.2 Classical Monte Carlo Simulation

The usual approach for Monte Carlo simulation of path-dependent options is the simulation of the whole path from  $t = 0$  to  $t = T$  on a grid of time step  $\Delta t$ : for each time step we simulate the evolution of the asset and the maximum (or minimum) value reached in the path is considered. Then, the option value is computed as the mean of the outcomes, one for each simulated path.

Let's consider the case of an underlying asset with dynamics given by the Geometric Brownian Motion in the risk-neutral measure with dividend yield:

$$dS_t = (r - q)S_t dt + \sigma S_t dW_t,$$

with  $r$  risk-free rate and  $q$  dividend yield, and  $W_t$  is a standard Brownian Motion. Then, the log-returns  $X_t = \log(S_t/S_0)$  follow the dynamics of a Brownian Motion with drift and diffusion:

$$dX_t = \left( r - q - \frac{\sigma^2}{2} \right) dt + \sigma dW_t, \quad X_0 = 0.$$

Consider the time grid  $t_k = k\Delta t$ , for  $k = 0, \dots, n$ , such that  $t_0 = 0$  and  $t_n = T$ ; on each time step, the Brownian Motion can be generated according to the following recursive formula:

$$X_{t_{k+1}} = X_{t_k} + \left( r - q - \frac{\sigma^2}{2} \right) \Delta t + \sigma \sqrt{\Delta t} Z_k,$$

where  $\{Z_k\}$  are i.i.d random variables with a standard normal distribution, i.e.  $Z \sim \mathcal{N}(0, 1)$ . Indeed, as for definition 4.1, the increments on disjoint intervals are independent. Then, calling the maximum and the minimum value of the log-returns:

$$\overline{X}_T = \max_{k=0, \dots, n} X_{t_k}, \quad \underline{X}_T = \min_{k=0, \dots, n} X_{t_k},$$

we get:

$$\overline{S}_T = \max_{k=0, \dots, n} S_{t_k} = S_0 e^{\overline{X}_T}, \quad \underline{S}_T = \min_{k=0, \dots, n} S_{t_k} = S_0 e^{\underline{X}_T}.$$

The value of the options is then computed as the mean on  $N$  paths of the possible outcomes, given a strike price  $K$  and a lower barrier  $B$ :

$$V_{fix}^{LC}(0) = e^{-rT} \frac{1}{N} \sum_{j=1}^N \max(\bar{S}_T^j - K, 0); \quad (4.1)$$

$$V^{D\&O}(0) = e^{-rT} \frac{1}{N} \sum_{j=1}^N \max(S_T^j - K, 0) \cdot I_T^j, \quad I_T^j = \begin{cases} 1, & \underline{S}_T^j \geq B \\ 0, & \underline{S}_T^j < B \end{cases} \quad (4.2)$$

The precision of the approximation increases with the number  $N$  of simulated paths, but also with the number of time steps  $n$  considered. The order of error convergence in this kind of simulation is  $\mathcal{O}(\Delta t^{1/2})$ . Another issue is that for a fixed time step  $\Delta t$ , the usual Monte Carlo method does not converge to the correct result, computed with the closed formula, since even if we can consider a very small  $\Delta t$ , the option we are pricing is discretely (and not continuously) monitored. For that reason, there's the need to find a new approach that allows us to converge to the exact result.

### 4.3 Distribution of the Extrema

The idea for a new method is to find a way to introduce the distribution of the extrema of the Brownian Motion process directly into the simulation, as this distribution is theoretically known. First, we derive the joint distribution of a standard Brownian Motion and its maximum; then, we present the extension to the more generic Brownian Motion with drift and diffusion; finally, we consider the distribution of the extrema for a Brownian Bridge.

#### 4.3.1 Joint Distribution of Brownian Motion and its Maximum

In order to get the distribution of the maximum for the Brownian Motion  $W_t$ , the Reflection Principle must be introduced:

**Theorem 4.1** (Reflection Principle). *Consider  $M_t = \sup_{s \in [0, t]} W_s$ , where  $W_t$  is a standard Brownian Motion and consider  $a > 0$ , then:*

$$\mathbb{P}(M_t \geq a) = 2\mathbb{P}(W_t \geq a).$$

The proof of this theorem implies the use of the hitting time  $\tau_a$  at which the Brownian Motion  $W_t$  takes value  $a$  and the fact that the two "reflected" paths at  $a > 0$  of the Brownian Motion after the instant  $\tau_a$  have the same probability to happen, i.e.:

$$\mathbb{P}(W_T < a | \tau_a < T) = \mathbb{P}(W_T > a | \tau_a < T) = \frac{1}{2}.$$

In a similar way, given  $b \in [0, a]$ :

$$\begin{aligned} \mathbb{P}(W_T < b | \tau_a < T) &= \mathbb{P}(W_T > 2a - b | \tau_a < T) \\ \Rightarrow \mathbb{P}(W_T < b, \tau_a < T) &= \mathbb{P}(W_T > 2a - b, \tau_a < T); \end{aligned}$$

moreover, since the events  $\{M_T \geq a\} = \{\tau_a < T\}$  are exactly the same:

$$\mathbb{P}(W_T < b, M_T \geq a) = \mathbb{P}(W_T > 2a - b, M_T \geq a),$$

and being  $2a - b \geq a$ , the relation  $\{W_T > 2a - b\} \supset \{M_T \geq a\}$  holds, therefore:

$$\mathbb{P}(W_T < b, M_T \geq a) = \mathbb{P}(W_T > 2a - b) = \frac{1}{\sqrt{2\pi T}} \int_{2a-b}^{+\infty} e^{-\frac{x^2}{2T}} dx.$$

Thus, that yields to the joint probability density function of the standard Brownian Motion and its maximum for  $0 \leq b \leq a$ :

$$f_{M_T, W_T}(a, b) = -d\mathbb{P}(W_T < b, M_T \geq a) = \sqrt{\frac{2}{\pi T}} \frac{2a - b}{T} e^{-\frac{(2a-b)^2}{2T}} \mathbb{1}_{a \geq b \vee 0}. \quad (4.3)$$

This is a well-known result. As last step, we want to derive the same expression for the general Brownian Motion with drift  $\mu$  and diffusion  $\sigma$ , for which we refer back to the book of Shreve (2004).

**Theorem 4.2.** *The joint distribution of the Brownian Motion with drift  $\mu$  and diffusion  $\sigma$ , i.e.  $X_T = \mu T + \sigma W_T$ , and its maximum  $\bar{X}_T$  is given by:*

$$f_{\bar{X}_T, X_T}(a, b) = e^{\frac{\mu}{\sigma^2} b - \frac{\mu^2}{2\sigma^2} T} \sqrt{\frac{2}{\pi \sigma^2 T}} \frac{2a - b}{\sigma^2 T} e^{-\frac{(2a-b)^2}{2\sigma^2 T}} \mathbb{1}_{a \geq b \vee 0}.$$

*Proof.* This result is the application of Th. 7.2.1 of Shreve (2004, p. 296), that gives the joint distribution function of a Brownian Motion with drift  $\alpha$ , i.e.  $\widetilde{W}_T = \alpha T + W_T$ , and its maximum  $\widetilde{M}_T$ :

$$f_{\widetilde{M}_T, \widetilde{W}_T}(a, b) = e^{\alpha b - \frac{1}{2}\alpha^2 T} \sqrt{\frac{2}{\pi T}} \frac{2a - b}{T} e^{-\frac{(2a-b)^2}{2T}} \mathbb{1}_{a \geq b \vee 0},$$

considering that  $X_T = \sigma \widetilde{W}_T$ ,  $\bar{X}_T = \sigma \widetilde{M}_T$  when we choose  $\alpha = \mu/\sigma$ , and therefore modifying the joint distribution accordingly.  $\blacksquare$

### 4.3.2 Brownian Bridge and its Extrema

The Brownian Bridge is a stochastic process obtained by taking the standard Brownian Motion  $W_t$  on  $t \in [0, 1]$  and conditioning on the event that the final value at  $t = 1$  is equal to 0 a.s..

**Definition 4.2** (Brownian Bridge). *A Brownian Bridge is a real-valued stochastic process  $\{B_t\}_{t \in [0,1]}$  such that:*

- $B_0 = B_1 = 0$  a.s.;
- $B_t$  is a Gaussian process;
- $\mathbb{E}[B_t] = 0, \quad \forall t \in [0, 1]$  and  $\text{cov}(B_s, B_t) = \min\{s, t\} - st, \quad \forall s, t \in [0, 1]$ ;
- $t \mapsto B_t$  is continuous a.s. on  $[0, 1]$ .

**Remark.** In the general case, the Brownian Bridge passing through  $B_{t_0} = x_0$  and  $B_{t_1} = x_1$  is a stochastic process with normal distribution with:

$$\mathbb{E}[B_t] = x_0 + \frac{t - t_0}{t_1 - t_0}(x_1 - x_0) \quad \text{and} \quad \text{cov}(B_s, B_t) = \frac{(t_1 - t)(s - t_0)}{t_1 - t_0}, \quad s < t.$$

It's possible to compute the probability distribution function for the maximum (or the minimum) of a Brownian Bridge, exploiting the formula we found in the previous paragraph and the properties of conditional distributions. Indeed, for continuous random variables the conditional probability distribution function on variable  $Y$  given the occurrence of  $X = x$  is given by:

$$f_{Y|X=x}(y) = \frac{f_{X,Y}(x, y)}{f_X(x)}.$$

We start from the Brownian Motion with drift and diffusion  $X_t = \mu t + \sigma W_t$ , with initial value  $X_0 = 0$  and maximum  $\bar{X}_t = \max_{s \in [0, t]} X_s$ ; it's even possible to consider the shifted process  $X_t^{(c)} = c + X_t$  that starts at  $X_0^{(c)} = c$ : the formulas will be the same, with just a change of variable to be applied; therefore, we proceed with  $X_t$  without loss of generality.

Consider a general bridge  $B_t$  generated by  $X_t$  between  $(0, 0)$  and  $(T, b)$ , i.e. the Brownian bridge generated considering the Brownian Motion with drift and diffusion  $X_t$  conditioning on the event  $\{X_T = b\}$ . The probability distribution function of the maximum  $\bar{B}_T = \max_{t \in [0, T]} B_t$  is given by:

$$f_{\bar{B}_T}(a) = f_{\bar{X}_T|X_T=b}(a) = \frac{f_{\bar{X}_T, X_T}(a, b)}{f_{X_T}(b)} = \frac{2(2a - b)}{\sigma^2 T} e^{-\frac{2(a^2 - ab)}{\sigma^2 T}} \mathbb{1}_{a \geq b \vee 0},$$

and the cumulative distribution function can be recovered by integration:

$$F_{\bar{B}_T}(y) = F_{\bar{X}_T|X_T=b}(y) = \int_{b \vee 0}^y \frac{2(2a - b)}{\sigma^2 T} e^{-\frac{2(a^2 - ab)}{\sigma^2 T}} da = (1 - e^{-\frac{2y(y-b)}{\sigma^2 T}}) \mathbb{1}_{y \geq b \vee 0}. \quad (4.4)$$

It's important to notice that the distribution of the maximum of the Brownian Bridge does not depend on the drift coefficient, but only on the diffusion parameter.

In a very similar way, it is also possible to compute the cumulative distribution function of the minimum  $\underline{B}_T = \min_{t \in [0, T]} B_t$  of the Brownian bridge generated by  $X_t$  conditioning on the final value  $X_T = b$ . Considering that the minimum  $\underline{X}_t = \min_{s \in [0, t]} X_s$  has the same distribution of  $\bar{X}_t - X_t$ , then one gets:

$$F_{\underline{B}_T}(y) = F_{\underline{X}_T|X_T=b}(y) = e^{-\frac{2y(b-y)}{\sigma^2 T}} \mathbb{1}_{y \leq b \vee 0}. \quad (4.5)$$

**Remark.** It is important to remark that here we are considering separately the the joint distribution of  $(X_T, \bar{X}_T)$  and the joint distribution of  $(X_T, \underline{X}_T)$ : this method can be used only in case of lookback or single barrier, while for a double barrier option one should consider the joint distribution of the three variables  $(X_T, \bar{X}_T, \underline{X}_T)$ , which involves a more sophisticated algorithm for the inversion of a series (see Becker (2010)). In this work, we stick to the simpler method since we are considering a lookback on the maximum and a single barrier option.

## 4.4 New Monte Carlo Simulation for the BM model

The idea for the improvement of the Monte Carlo Simulation method is to use the distribution of the maximum or of the minimum computed in the previous paragraph. Indeed, when we simulate the path of the Brownian Motion, we generate a certain number  $n = T/\Delta t$  of points  $\{x_i\}_{i=1,\dots,n}$ , where  $x_i$  is the simulated value of  $X_{t_i}$ . Now, let's consider to start from this simulation: given the couples  $(t_i, x_i)$ ,  $\forall i = 0, \dots, n$ , we want to study the stochastic process  $X_T$  that is a concatenation of  $n$  independent Brownian Bridges  $\{B_s^i\}_{s \in [t_{i-1}, t_i]}$  passing through  $B_{t_{i-1}} = x_{i-1}$  and  $B_{t_i} = x_i$ . Instead of taking the maximum (or the minimum) of the simulated  $x_i$  directly, on each interval  $[t_{i-1}, t_i]$  we generate the maximum according to the distribution (4.4) and the minimum according to (4.5). Therefore, calling  $\overline{B}_i = \max_{s \in [t_{i-1}, t_i]} B_s^i$  and  $\underline{B}_i = \min_{s \in [t_{i-1}, t_i]} B_s^i$ , for each bridge we have:

$$F_{\overline{B}_i}(y) = \left(1 - e^{-\frac{2(y-x_i)(y-x_{i-1})}{\sigma^2 \Delta t}}\right) \mathbb{1}_{y \geq \max(x_{i-1}, x_i)},$$

$$F_{\underline{B}_i}(y) = e^{-\frac{2(x_i-y)(x_{i-1}-y)}{\sigma^2 \Delta t}} \mathbb{1}_{y \leq \min(x_{i-1}, x_i)}.$$

Moreover, we know that every cumulative distribution function takes values in  $[0, 1]$ , thus, generating a uniform random variable  $u_i$  on  $[0, 1]$  for each interval, knowing the initial point  $x_{i-1}$  and the final point  $x_i$ , the simulated maximum  $\overline{x}_i$  and the simulated minimum  $\underline{x}_i$  for interval  $[t_{i-1}, t_i]$  are computed as:

$$\overline{x}_i = F_{\overline{B}_i}^{-1}(u_i) = \frac{1}{2}(x_i + x_{i-1} + \sqrt{(x_i - x_{i-1})^2 - 2\sigma^2 \Delta t \log(1 - u_i)}), \quad (4.6)$$

$$\underline{x}_i = F_{\underline{B}_i}^{-1}(u_i) = \frac{1}{2}(x_i + x_{i-1} - \sqrt{(x_i - x_{i-1})^2 - 2\sigma^2 \Delta t \log(u_i)}), \quad (4.7)$$

Therefore, the total maximum and minimum on  $[0, T]$  are given by:

$$\overline{X}_T = \max_{i=1,\dots,n} \overline{x}_i, \quad \underline{X}_T = \min_{i=1,\dots,n} \underline{x}_i.$$

Finally, the maximum or minimum value for the underlying asset  $S_T$  are recovered as:

$$\overline{S}_T = S_0 e^{\overline{X}_T}, \quad \underline{S}_T = S_0 e^{\underline{X}_T}.$$

Performing the simulation for  $N$  different paths, the options' prices are obtained applying formulas (4.1) and (4.2).

### 4.4.1 Numerical results

In this paragraph, we compare the convergence of the classical and of the new Monte Carlo method to the exact result of the closed formula. As said, the fact of using directly the known distribution of the extrema will led to an higher order of convergence with respect to the thickness of the simulation grid  $\Delta t$  and also to an actual convergence to the correct value with the increasing of the number of simulations. We apply the new method assuming a Brownian Motion model for the log-returns: the results for both the Fixed Strike Lookback call option and the Single Barrier Down & Out call option are presented.



## Convergence with the grid

First, let's recall that the option we are going to price is a path-dependent option: this means that we are interested not only in the final asset value at maturity  $T$ , but also in the intermediate values. In this first analysis, we want to check how the method converges to the exact result as the number of points in the time grid increases, i.e. as  $\Delta t$  decreases. In order to kill the noise of the Monte Carlo variability with  $N$  paths and consider only the convergence for  $\Delta t$ , we consider the same  $N$  simulated paths for every  $\Delta t$ . In order to do so, for each path  $j$  we first simulate the path with the smallest  $\Delta t_{\min}$  considered, in the application  $\Delta t_{\min} = 2^{-8}$ ; then, we derive the path for a bigger  $\Delta t$  picking the points of the thicker path. Figure 4.1 can provide an idea of the procedure.

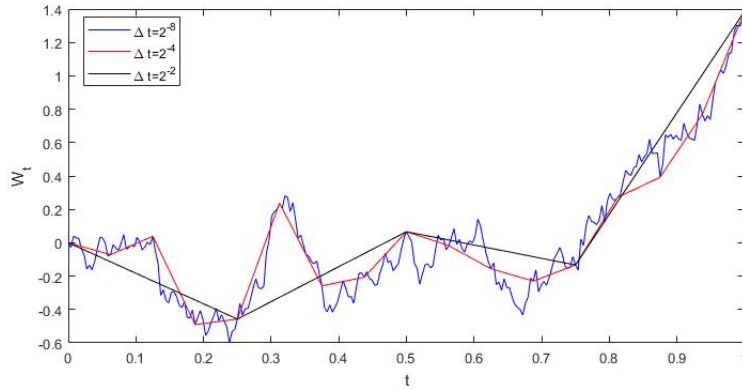


Figure 4.1: Path of a standard Brownian Motion  $W_t$  between  $[0, 1]$  with different time steps.

In this way, we can capture the effect of changing the grid's step size in the two different Monte Carlo methods by simply computing the absolute error:

$$\hat{\epsilon}_{\Delta t}^N = \left| \sum_{j=1}^N V_{\Delta t}^j - V_{CF} \right|,$$

where  $V_{\Delta t}^j$  is the option price for path  $j$ . In order to see the effect of the method, we should choose smartly the parameters: while for the lookback option the result is highly dependent on the value of the maximum, the single barrier's price is affected by the value of the minimum only through the indicator  $I_T$  of formula (4.2). Therefore, the greatest difference in price between a plain vanilla option and a barrier option is just in the neighborhood of the barrier. For that reason, we choose an initial spot  $S_0 = 0.81$  near to the barrier, and the other parameters as in chapter 3.

The absolute error embedded in the Classical Monte Carlo method is represented by the red line: in figure 4.2 it is possible to see that the convergence is slightly slower than  $\mathcal{O}(\Delta t^{\frac{1}{2}})$  (the black dotted line), while the blue line represents the New Monte Carlo method with simulation of the maximum or the

minimum between time steps: the speed of convergence is way higher, even if it doesn't reach the speed of  $\mathcal{O}(\Delta t)$ .

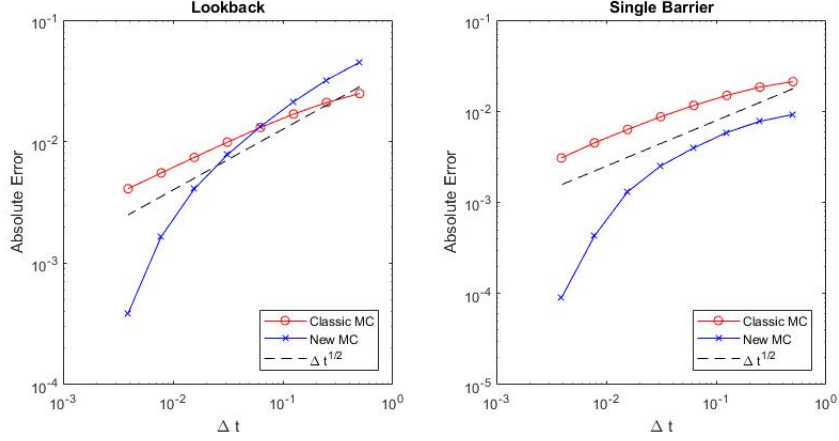


Figure 4.2: Comparison of the convergence of the absolute error w.r.t.  $\Delta t$  of the two Monte Carlo methods in log-log scale under the BM model. Results obtained with  $N = 4 \cdot 10^5$  simulations, for  $\Delta t = 2^{-1}, \dots, 2^{-8}$ .

### Convergence with the number of simulations

Probably the greatest improvement of this method is in the convergence of the absolute error with respect to the number of simulations used. The usual Monte Carlo has a great issue, which is, for a given  $\Delta t$ , not to converge to the exact result. The reason of this behaviour is that we are actually pricing a different option: not a continuously, but a discretely monitored one, which has a different price. Therefore there's a limit to which the simulation can converge to the right result, because of the granularity of the grid: for example, in the lookback option we always take as maximum value one of the asset's values among a discrete number of points, but we don't know what happens in between. On the other hand, in the new method we can simulate the position of the maximum: in this way, the convergence to the exact result is granted, because we are using directly the distribution of the maximum. The same applies in the single barrier case. Therefore, first we check that the new method actually converges, comparing the mean of the absolute error of the classic and the new method with respect to the exact solution as  $N$  increases; then, we analyze the order of magnitude of the error with the estimator of the Monte Carlo noise.

The first error estimate is computed as the mean of absolute errors, therefore we first have to compute the option price as a mean of  $N$  simulated payout, then we have to take the mean of  $M$  absolute errors, i.e.:

$$\hat{\epsilon}_{Abs} = \sum_{k=1}^M \left| \sum_{j=1}^N V_{j,k} - V_{CF} \right|,$$

where  $V_{j,k}$  is the option price for path  $j$  of bunch  $k$ . Selecting the parameters as before, we notice in figure 4.3 that as expected the classic Monte Carlo does

not converge to the closed formula result, while the new method guarantees the convergence of the absolute error.

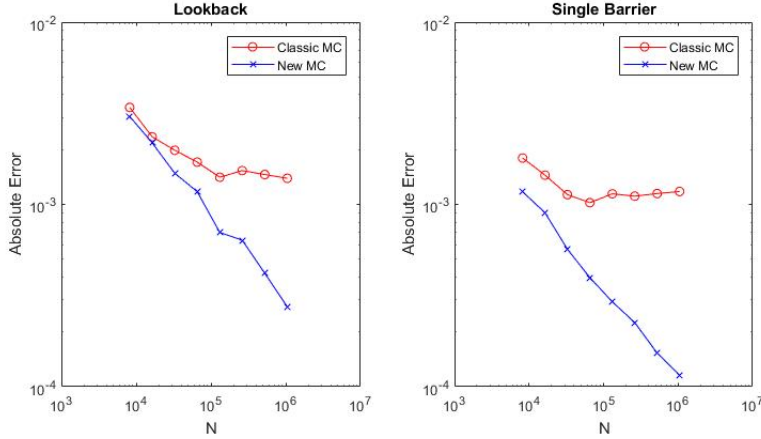


Figure 4.3: Comparison of the mean of the absolute error w.r.t the number of simulations  $N$  of the two Monte Carlo methods in log-log scale under the BM model. Results obtained for  $N = 2^7, \dots, 2^{14}$  simulations for  $M = 2^6$  bunches with  $\Delta t = 2^{-7}$ .

Once we have checked that the new Monte Carlo actually converges, in order to have a better estimate of the rate of convergence we use as estimator the expression:

$$\hat{\epsilon}_{\Delta t}^N = \hat{\sigma}_{\Delta t}^N = \sqrt{\frac{\text{Var}(V_{\Delta t}^j)}{N}}, \quad (4.8)$$

where  $\text{Var}(x^j)$  is the variance of sample  $\{x^j\}_{j=1, \dots, N}$ . In this way, we can exploit all the simulations (up to  $N = 2^{20} \approx 10^6$  with  $\Delta t = 2^{-8}$ ) to estimate the error. In figure 4.4, it is possible to see that the described methodology reaches the usual Monte Carlo rate of convergence of  $\mathcal{O}(1/\sqrt{N})$ .

## 4.5 New Monte Carlo Simulation for NIG Model

The Monte Carlo simulation for a process with dynamics following a Normal Inverse Gaussian model is a bit more complicated than the simple Brownian Motion with drift and diffusion used in the previous section. Indeed, this kind of process may be seen as a subordinated Brownian Motion, i.e. a Brownian Motion combined with an Inverse Gaussian (IG) process. First, let's have an overview about how it is possible to simulate such a process; then we will see how to apply the new approach for the simulation of the extrema.

Following the approach of Webber and Ribeiro (2003), we define the Normal Inverse Gaussian (NIG) process  $X_t$  as a Lévy process where the increments are distributed according to the NIG distribution. The process is defined by the

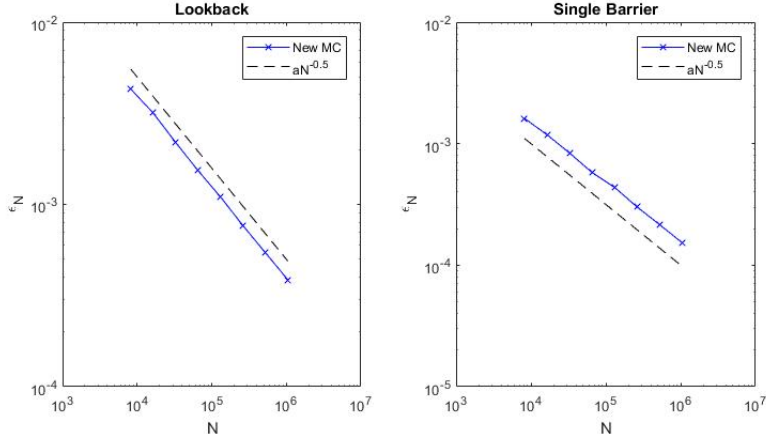


Figure 4.4: Convergence of the Monte Carlo error estimate w.r.t the number of simulations  $N$  of the new Monte Carlo method in log-log scale under the BM model. Results obtained for  $N = 2^{13}, \dots, 2^{20}$  simulations with  $\Delta t = 2^{-8}$ .

parameters  $(\alpha, \beta, \delta, \mu)$ , with characteristic exponent:

$$\psi_{NIG}(z) = i\mu z + \delta(\gamma - \sqrt{\alpha^2 - (\beta + iz)^2}),$$

where  $\gamma = \sqrt{\alpha^2 - \beta^2}$ , with  $\delta > 0$  and  $0 \leq |\beta| \leq \alpha$ . For the application to option pricing, the NIG process  $X_t$  can be written as:

$$X_t = \mu t + W_{h(t)},$$

where  $W_t$  is a Brownian Motion with drift  $\beta$  and variance 1, while  $h(t)$  is an Inverse Gaussian process with parameters  $(\delta t, \gamma)$ . Moreover, if  $X_t$  represents the log-return of an underlying asset  $S_t$  with risk-free rate  $r$  and dividend yield  $q$ , then the risk-neutral measure is recovered choosing:

$$\mu = r - q - \delta(\gamma - \sqrt{\alpha^2 - (\beta + 1)^2}).$$

and finally  $S_t = S_0 e^{X_t}$ . In order to construct a discrete sample path for the subordinated Brownian Motion  $W_{h(t)}$ , first simulate the Inverse Gaussian discrete process  $\{h_k\}$  on the grid  $t_k = k\Delta t$ , for  $k = 0, \dots, n$ , such that  $t_0 = 0$  and  $t_n = T$ , where the increments are computed as:

$$\Delta h_k = h_k - h_{k-1} \sim IG(\delta \Delta t, \gamma), \quad h_0 = 0.$$

Then, simulate a discrete Brownian Motion  $\{W_k\}$  with increments sampled as:

$$\Delta W_k = W_k - W_{k-1} \sim \mathcal{N}(\beta \Delta h_k, \Delta h_k), \quad W_0 = 0.$$

Finally, the required discrete NIG process  $\{X_k\}$  is given by:

$$X_k = \mu t_k + W_k, \quad \text{for } k = 0, \dots, n.$$

The classic Monte Carlo simulation for extrema would sample:

$$\bar{X}_T = \max_{k=0, \dots, n} X_k, \quad \underline{X}_t = \min_{k=0, \dots, n} X_k.$$

In order to introduce the new approach, let's notice that the increment  $\Delta h_k$  is basically the variance of the increment  $\Delta W_k$  on the interval  $[t_{k-1}, t_k]$ : therefore, once we have the points on the grid  $(t_k, X_k)$ , we can simply apply formulas (4.6) and (4.7) taking for each time interval  $[t_{k-1}, t_k]$  the diffusion  $\sigma = \sqrt{\Delta h_k}$ .

### 4.5.1 Numerical Results

The comparison with an exact reference value in this case is impossible, since the closed formulas for lookback and barrier options are available only in the Brownian Motion case. Therefore, in order to judge the convergence of the method, we compare the results obtained via Monte Carlo with the ones obtained via the analytical Wiener-Hopf method. Indeed, the analysis of the previous chapter on the results of the method shows that the error made at  $S_0 = 0.81$  with grid size  $2^{16}$  is smaller than  $10^{-4}$  (see figure 3.10). Therefore, we can use this as a reference value, being the Monte Carlo error greater than  $10^{-4}$  with the number of simulations we are running. The choice of parameters for the NIG distribution has been made following Phelan et al. (2018), as in chapter 3.

In figure 4.5 and 4.6, we can see that the convergence is similar to the one obtained in the Brownian Motion case. Only on the last step we reach an error which is comparable to the one of the analytic method, therefore the lack of convergence in the last step of figure 4.5 is due to the fact that we are not comparing the Monte Carlo method with an exact value.

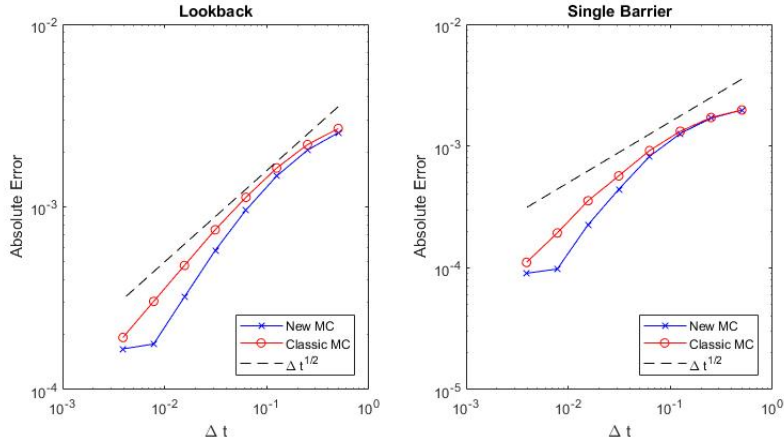


Figure 4.5: Comparison of the convergence of the absolute error in  $\Delta t$  of the two Monte Carlo methods in log-scale under NIG model. Results obtained with  $N = 2 \cdot 10^5$  simulations, for  $\Delta t = 2^{-1}, \dots, 2^{-8}$ .

The rate of convergence of the new method, as in the Brownian Motion case, doesn't need the reference value to be checked, since we can estimate it directly from the sample with equation (4.8). As it is possible to see in figure 4.7, also in the NIG model case the method is convergent with  $\mathcal{O}(1/\sqrt{N})$ .

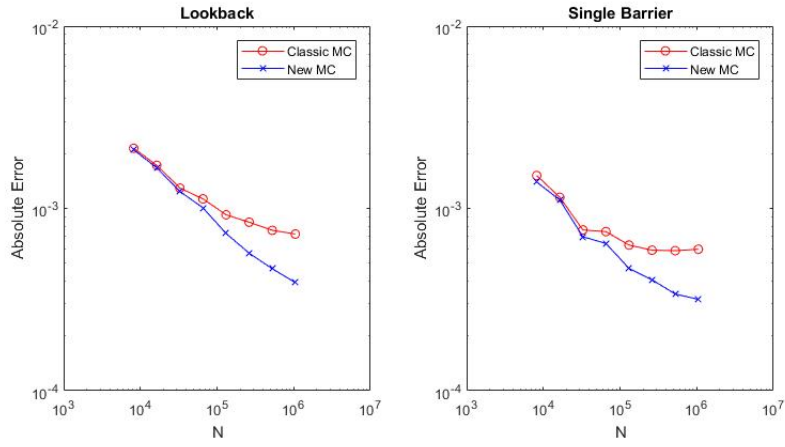


Figure 4.6: Comparison of the mean of the absolute error w.r.t the number of simulations  $N$  of the two Monte Carlo methods in log-scale under NIG model. Results obtained for  $N = 2^7, \dots, 2^{14}$  simulations for  $M = 2^6$  bunches with  $\Delta t = 2^{-5}$ .

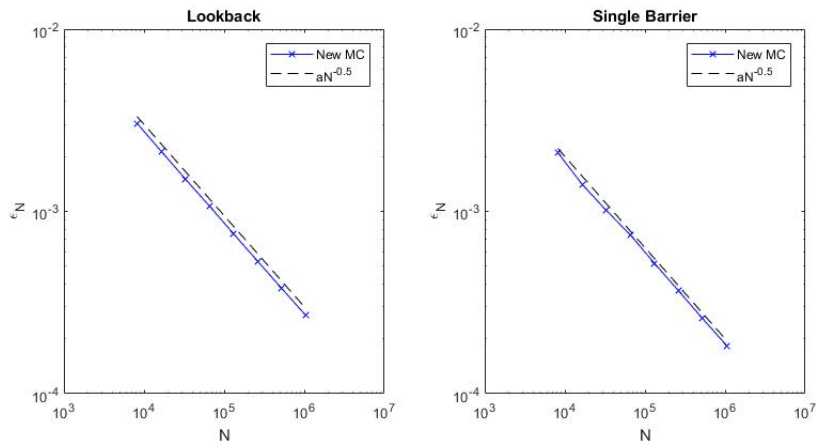


Figure 4.7: Convergence of the Monte Carlo error estimate w.r.t the number of simulations  $N$  of the new Monte Carlo method in log-scale under NIG model. Results obtained for  $N = 2^{13}, \dots, 2^{20}$  simulations with  $\Delta t = 2^{-8}$ .

# Chapter 5

## Conclusions

In this work we have presented two different approaches for the pricing of continuously monitored exotic options under Lévy models: the Wiener-Hopf method and the modified Monte Carlo.

The first is an analytical method, that relies on numerical techniques for the computation of the integrals inside the formulas. It makes use of advanced mathematical techniques, such as the Wiener-Hopf technique or the Inverse Laplace Transform; moreover, the numerical computations involved require a deep comprehension of the methods and a discussion about their convergence. The application of such decomposition to option pricing has been studied in the literature, such as in Phelan et al. (2018), but even before in Sgarra et al. (2006). Thanks to that, it is possible to rely on different works for the analysis of the many numerical methods and of the different analytical approaches, since each work focuses on a piece of the puzzle. For example, in Phelan et al. (2017) we have a deep study of the Hilbert transform, while Green et al. (2010) describes in details the Wiener-Hopf decomposition. One of the most important analysis is in Feng and Linetsky (2008), since it studies the analyticity strips in which it is possible to choose the damping parameter for many different Lévy processes. The main contribution of this thesis is the application of the technique for continuously monitored options to Lookback options and for the American and Barrier Digital options. Moreover, the presence of an analyticity region for the method has been analyzed, focusing on both the mathematical settings, with the graphical study on the Hilbert Transform of the function to be decomposed (section 3.3), and the numerical evidence on the region for the damping parameter (section 3.4).

In this thesis we also consider a method which is completely numerical. It relies only on the mathematical derivation of the distribution of the maximum for the Brownian Motion and its application to the classical Monte Carlo approach. For that reason, the proposed modified Monte Carlo method is very easy to implement and, differently from the first method, is not based on complicated mathematical techniques. In addition, it shows nice convergence properties that are usually not satisfied by the classical simulation procedure. On this side, the literature is richer on Brownian Motion (e.g. see Alabert and Caballero (2018) and Becker (2010)). In this thesis, the financial application involves two dif-

ferent models for the log-returns of the underlying asset: the Brownian Motion model, used basically as a control thanks to the presence of closed formulas, and the Normal Inverse Gaussian Model. The new feature introduced is the modified Monte Carlo simulation for the NIG model.

The results obtained highlight that the two methods are actually comparable regarding the possibility of application and the power of convergence. Indeed, for both the methods the option price computed shows an error approximately of  $\mathcal{O}(10^{-4})$ ; moreover, both have been applied to single barrier options and lookback options.



## Notation

Symbol	Description
$\mathbb{1}$	Indicator Function
$\Re$	Real Part
$\Im$	Imaginary Part
$\Psi$	Characteristic Function of a Lévy Process
$\psi$	Characteristic Exponent of a Lévy Process
$\hat{f}(z), \mathcal{F}$	Fourier Transform
$\tilde{f}(s), \mathcal{L}$	Laplace Transform
$\mathcal{H}$	Hilbert Transform
$\hat{f}_{\pm}(z)$	Half-range Fourier Transform, Wiener-Hopf factors
$\mathcal{Z}$	Zeta (Z-) Transform
$\text{sgn}(x)$	Sign function
$\text{rect}(x)$	Rectangular function
$\text{sinc}(x)$	Sinc function
$S_t$	Spot price at time t
$\overline{S}_t, \underline{S}_t$	maximum and minimum of $S_t$
$X_t$	Log-return, Lévy Process at time t
$\overline{X}_t, \underline{X}_t$	maximum and minimum of $X_t$
$V.(0)$	Option price at time $t = 0$
$r$	Risk-free rate
$q$	Dividend Yield
$K$	Strike Price
$B$	Barrier Level
$\phi(x), \phi_{\gamma}(x)$	Payoff function, damped payoff function
$\gamma$	Damping Parameter
$N$	Number of grid points for FFT
$\Delta z$	Step size in the transformed space
$\Delta x$	step size in the real space
$\{x_l\}$	points of the grid in the real space
$\{z_j\}$	points of the grid in the transformed space
$\{s_k\}$	points for the trapezoidal method
$\sigma(\cdot)$	Exponential filter
$A$	Trapezoidal rule parameter
$m_E, n_E$	Euler acceleration parameters
$W_t$	Brownian Motion
$M_t$	Maximum of the Brownian Motion
$B_t$	Brownian Bridge
$\overline{B}_t, \underline{B}_t$	maximum and minimum of the Brownian Bridge
$(\mu, \sigma)$	Parameters of Brownian Motion Model
$(\alpha, \beta, \delta, \mu)$	Parameters of Normal Inverse Gaussian Model
i.i.d	independent and identically distributed
w.r.t	with respect to
FFT	Fast Fourier Transform
NIG	Normal Inverse Gaussian
BM	Brownian Motion
IG	Inverse Gaussian
ATM	At-The-Money option

# Bibliography

- Abate, Joseph and Ward Whitt (1992). “The Fourier-series method for inverting transforms of probability distributions”. In: *Queueing systems* 10.1-2, pp. 5–87.
- (1995). “Numerical inversion of Laplace transforms of probability distributions”. In: *ORSA Journal on computing* 7.1, pp. 36–43.
- Alabert, Aureli and Ricard Caballero (2018). “On the minimum of a conditioned Brownian bridge”. In: *Stochastic Models*, pp. 1–23.
- Arfken, G (1985). “Mathematical Methods for Physicists 3rd edn (Orlando, FL: Academic)”. In:
- Baxter, Glen and Monroe D Donsker (1957). “On the distribution of the supremum functional for processes with stationary independent increments”. In: *Transactions of the American Mathematical Society* 85.1, pp. 73–87.
- Becker, Martin (2010). “Exact simulation of final, minimal and maximal values of Brownian motion and jump-diffusions with applications to option pricing”. In: *Computational Management Science* 7.1, p. 1.
- Carr, Peter and Dilip Madan (1999). “Option valuation using the fast Fourier transform”. In: *Journal of computational finance* 2.4, pp. 61–73.
- Feng, Liming and Vadim Linetsky (2008). “Pricing discretely monitored barrier options and defaultable bonds in Lévy process models: a fast Hilbert transform approach”. In: *Mathematical Finance: An International Journal of Mathematics, Statistics and Financial Economics* 18.3, pp. 337–384.
- Fusai, Gianluca, Guido Germano, and Daniele Marazzina (2016). “Spitzer identity, Wiener-Hopf factorization and pricing of discretely monitored exotic options”. In: *European Journal of Operational Research* 251.1, pp. 124–134.
- Gottlieb, David and Chi-Wang Shu (1997). “On the Gibbs phenomenon and its resolution”. In: *SIAM review* 39.4, pp. 644–668.
- Green, Ross, Gianluca Fusai, and I David Abrahams (2010). “The Wiener-Hopf technique and discretely monitored path-dependent option pricing”. In: *Mathematical Finance: An International Journal of Mathematics, Statistics and Financial Economics* 20.2, pp. 259–288.
- King, Frederick W (2009). *Hilbert transforms*. Vol. 1. Cambridge University Press Cambridge.
- Kisil, Anastasia V (2015). “The relationship between a strip Wiener–Hopf problem and a line Riemann–Hilbert problem”. In: *IMA Journal of Applied Mathematics* 80.5, pp. 1569–1581.
- Lawrie, Jane B and I David Abrahams (2007). “A brief historical perspective of the Wiener–Hopf technique”. In: *Journal of Engineering Mathematics* 59.4, pp. 351–358.

- Lewis, Alan L (2001). “A simple option formula for general jump-diffusion and other exponential Lévy processes”. In: *Available at SSRN 282110*.
- Phelan, Carolyn E, Daniele Marazzina, Gianluca Fusai, and Guido Germano (2017). “Hilbert transform, spectral filtering and option pricing”. In: *arXiv preprint arXiv:1706.09755*.
- (2018). “Fluctuation identities with continuous monitoring and their application to the pricing of barrier options”. In: *European Journal of Operational Research* 271.1, pp. 210–223.
- Sgarra, Carlo, Gianluca Fusai, and I David Abrahams (2006). “An exact analytical solution for discrete barrier options”. In: *Finance and Stochastics* 10.1, pp. 1–26.
- Shreve, Steven E (2004). *Stochastic calculus for finance II: Continuous-time models*. Vol. 11. Springer Science & Business Media.
- Spitzer, Frank (1956). “A combinatorial lemma and its application to probability theory”. In: *Transactions of the American Mathematical Society* 82.2, pp. 323–339.
- Stenger, Frank (2000). “Summary of Sinc numerical methods”. In: *Journal of Computational and Applied Mathematics* 121.1-2, pp. 379–420.
- Stenger, Frank and Kelly M McArthur (1994). “Numerical Methods Based on Sinc and Analytic Functions”. In: *SIAM Review* 36.4, pp. 673–673.
- Webber, Nick and Claudia Ribeiro (2003). *A Monte Carlo method for the Normal Inverse Gaussian option valuation model using an Inverse Gaussian bridge*. Tech. rep. Society for Computational Economics.
- Wendel, JG (1958). “Spitzer’s formula: a short proof”. In: *Proceedings of the American Mathematical Society* 9.6, pp. 905–908.